Aalto University
School of Electrical
Engineering

AALTO UNIVERSITY
SCHOOL OF ELECTRICAL ENGINEERING

Department of Electrical Engineering

Bishal Silwal

Computation of eddy currents in a solid rotor induction machine with 2-D and 3-D FEM

Thesis supervisor:
Professor Antero Arkkio

Thesis instructor:
Docent Anouar Belahcen

AALTO UNIVERSITY

SCHOOL OF ELECTRICAL ENGINEERING Abstract of the Master's Thesis

Author: Bishal Silwal

Name of the topic: Computation of eddy currents in a solid rotor induction machine with 2-D and 3-D FEM

Date: 24.04.2012 Language: English Number of pages: ix+62

Department of Electrical Engineering

Professorship: Electromechanics Code: S-17

Supervisor: Professor Antero Arkkio

Instructor: Docent Anouar Belahcen

Abstract

Although a two-dimensional numerical analysis of an electrical machine provides an approximately accurate solution of the electromagnetic field in the machine, a three-dimensional study is needed to understand the actual phenomena. But due to the large problem size and the complex geometries, the three dimensional model requires a huge amount of degrees of freedoms (DoFs) to be solved, which is not possible with a limited computing resources. Therefore, a coupled 2D-3D model can be the best alternative to solve such type of problems.

In this thesis, a 2-D finite element analysis is performed on a solid rotor induction motor by an in-house software FCSMEK. The eddy current in the solid steel rotor was computed. A 3-D model for the same machine was built and solved in COMSOL Multiphysics™. To reduce the computation time of the 3-D model, the solution of the 2-D model was used as the source to the 3-D model where the stator current density is used as a transferred variable. The eddy currents are computed and the results from both 2-D and 3-D simulations are compared. Other quantities of interest such as the torque of the machine computed with the 2-D and 3-D models are also computed and compared.

Keywords: Electrical Machines, Finite Element Method (FEM), Eddy Currents, Coupled Models

ACKNOWLEDGEMENT

My master's thesis is a part of a research project that is funded by the Academy of Finland. Firstly, I am indebted to my instructor Dr. Anouar Belahcen for his support, encouragement, ideas and advice ranging from the minute technical details to the overall research process. His guidance helped me to learn a lot from this project. A sincere thanks goes to my supervisor Prof. Antero Arkkio for his support and motivation through-out the research process. A share of thanks goes to the Head of the Department of Electrical Engineering Prof. Asko Niemenmaa for creating a good working and research environment.

I would also like to express my gratitude to Mr. Ari Havisto for helping me by managing all the technical resources required for this thesis. I would also like to thank other members of the Electromechanic Research group such as Javiar Martinez, Paavo Rasilo, Van Khang Huynh, Mikko Heino and Ansi Sinvervo, with whom I have had many productive discussions. I heartily thank Deepak Singh and Tuomas Janhunen for their support and ideas that helped me a lot during the simulations.

I would also like to thank all the members of the Nepalese community here at Aalto University for always making this place a lively place to live in. Special thanks to Subash Khanal for helping me during the tough days.

Last but not least, I express my sincere gratitude to my parents Mr. Niranjan Silwal and Mrs. Janaki Silwal, my sisters Sanju, Ranju and Bijita and other relatives for their care, support and love, and also to my girlfriend Neha for her love, support and for understanding me and also for being very inquisitive about what I was doing.

Espoo, April 24, 2012

Bishal Silwal

TABLE OF CONTENTS

LIST OF FIGURES

LIST OF SYMBOLS AND ABBERVIATION

δ	Lamination Thickness
ε	Permittivity
μ	Magnetic Permeability
ρ	Electric Charge Density
σ	Conductivity
φ	Reduced Electric Scalar Potential
ψ	Reduced Magnetic Scalar Potential
ω_r	Angular Speed of Rotor
ω_s	Angular Speed of Stator
Ω	Magnetic Scalar Potential
$\boldsymbol{A}$	Magnetic Vector Potential
$\boldsymbol{B}$	Magnetic Flux Density
f	Frequency
$\boldsymbol{E}$	Electric Field Strength
$\boldsymbol{H}$	Magnetic Field Strength
I	Current
$\boldsymbol{J}$	Current Density
n	Rotor Speed
n_s	Synchronous Speed
P_e	Eddy Current Loss
P_h	Hysteresis Loss
R	Resistance
s	slip
$\boldsymbol{T}$	Electric Vector Potential
V	Voltage
V	Electric Scalar Potential
BEM	Boundary Element Method
CAD	Computer Aided Design

FEM	Finite Element Method
FDM	Finite Difference Method
PDE	Partial Differential Equation
rpm	Revolution per Minute
rps	Revolution per Second
THA	Time-Harmonic Analysis
TSA	Time-Stepping Analysis

~ CHAPTER 1 ~

INTRODUCTION

1.1 Background

Machines have always made life simpler, directly or indirectly. The development of an electrical machine began when Michael Faraday first demonstrated the conversion of electrical energy to mechanical energy through electromagnetic field in 1821. Since then numerous researches were done all around the globe to develop and apply electrical machines to make things easier, and today we stand where various ac and dc machines have been developed for a wide range of applications.

For the performance analysis of any machine, one important parameter to be considered is the machine loss. This consideration has significances like determining the efficiency of the machine which in turn influences the operating cost, determining the heating of machine which gives the machine rating without the deterioration of insulation, and for accounting the voltage drops or current component associated with the cause of the losses. Losses in electrical machines can be categorized according to the causes or phenomena that produce them. For instance, the Copper Loss or Ohmic Loss is the I^2R loss caused when a current I flows through the winding (copper in most cases) having a resistance R. The losses due to the friction in the brushes and bearing and windage losses are altogether considered to be the mechanical losses. The friction and windage losses can be measured by determining the unloaded and unexcited machine input at proper speed but generally they are lumped with core loss and determined at the same time. The Stray Load Loss is one kind of losses in electrical machines that arises from the non-uniform distribution of current in winding and the additional core losses produced in the iron due to the distortion of the magnetic flux caused by the load current. One major loss that highly affects the performance of the machine is the Core Loss. As the name depicts, it is the loss that occurs in the core of the machine, generally the iron part. In simple words, it is caused due to the

presence of time varying i.e. pulsating or rotating magnetic field in the magnetic material. Generally, there are two kinds of core losses. The first one being hysteresis loss, which is the loss because of the hysteresis produced by time varying magnetic field in the magnetic material. The hysteresis loss is proportional to the area of the hysteresis loop of the material and frequency. It is often expressed mathematically by an empirical relation which is also suggested by Fitzgerald and Kingsley (1961) and many other literatures after that.

$$P_h = K_h f B_{max}^n,$$

where K_h is a constant dependent on the characteristics of material and the exponent n ranges from 1.5 to 2.5.

The second kind of core loss is the eddy current loss. When a conductor is placed in a changing magnetic field, due to the relative motion of field and the conductor or the time variation of magnetic field, a current is induced in the conductor, which circulates over the conductor body. These circulating currents cause heating in the conductor core and also induces magnetic field which may oppose or add to the original field. It also causes the skin effect which is the phenomena where the current density is distributed towards the peripheral surface of the conductor. The eddy current loss varies with the square of the flux density, the frequency, and the thickness of the lamination. Under normal condition, the eddy current loss can be approximately expressed as suggested by Fitzgerald and Kingsley (1961) and also many other literatures after that, such that

$$P_e = K_e (B_{max} f \delta)^2,$$

where K_e is the proportionality constant, B_{max} is the maximum flux density, f is the frequency and δ is the lamination thickness.

Due to its robustness, ease of operation, reliability, durability and low maintenance cost, induction motor has found a wide range of industrial application. Moreover, there are many applications where a high speed induction machine is preferred. In this regard, solid rotor induction machines have been developed which eliminate the existence of mechanical gearbox in the machine, thus tending to increase the speed. The solid rotor induction machine operates on

the same principle as that of conventional induction machines, but the physical construction is different. Solid rotor is made up of a solid ferromagnetic body, for example steel, and does not have any windings. The strong mechanical strength of the solid rotor and its simple construction are also the prime reason of the use of solid rotor machines in high speed applications. But, its lower efficiency and power density play a vital role to degrade the machines performance where the induced eddy currents in the ferromagnetic rotor body add more into it. In recent years, research has been focused on the improvement of the efficiency of the high-speed solid rotor machine. According to Huppunen (2004) it has been found that a perfect sinusoidal flux density distribution on the rotor surface produces the lowest possible losses in the solid rotor high speed machines and therefore flux density distribution must be taken into important consideration in case of such machines. The fact that the smooth solid rotor runs at quite a low per-unit slip indicates that the efficiency of the machine can possibly be increased by reducing the stator and rotor losses as well as the harmonic content of the air-gap flux.

The accuracy and precision of the study of any electrical machine highly depends on what dimensional study we perform. So far both two dimensional and three dimensional analyses of machines are in existence. The two dimensional analysis is regarded to be simple and having low computational time because of relatively lower number of unknown variables to be solved. However for understanding of the exact phenomena, a three dimensional study of the machine is considered which is relatively complex with respect to the two dimensional computation. If we consider the numerical model or numerical analysis of the machine, the three dimensional computation of the solution by taking into account the coupled equations of different variables has not been reasonably possible. This is due to the large amount of unknown variables it has to solve. This problem is expected to be solved by a coupled two dimensional and three dimensional model. It can be expected that this kind of coupled model is not only relatively fast to solve because of the reduced number of unknowns but also gives an accurate result within given computational resources. One example of such coupling can be the coupling between the 2D model of the stator and a 3D finite element model of the rotor of an induction machine, where the eddy currents induced in the rotor has to be investigated as explained by Dziwniel et al. (1999).

This thesis is about the analysis of similar coupled two dimensional and three dimensional model of a solid steel rotor high speed machine. The research work is based on the coupling between the 2D model of the stator of the solid steel rotor high speed machine with the 3D model of its rotor and is focused on the computation of eddy currents in the rotor. The eddy currents will be computed from the 2D simulation, and the same field solution result from the 2D analysis will be used as a source to the 3D model of the rotor. The solution from the 2D and 3D simulations will be compared. This will not only help to analyze the eddy current loss distribution in the rotor surface but also assist to predict the performance of machine under given load condition.

1.2 Objectives

This project deals with the study of the solid steel rotor high speed machine, the study being based on the coupling between the 2D models of the stator of the machine with the 3D model of its rotor to accurately investigate eddy currents in the solid rotor parts without a need for a 3D model of the stator. The primary objectives of the project can be listed as follows:

i. To study about different magneto-dynamic models in electromechanics and various eddy current formulations in different dimension; literature review.
ii. To compute two dimensional field solution of the machine in an in-house software.
iii. To construct a 3D model of the machine to be used for computation in a commercial software.
iv. To use the two dimensional solution from the in-house software as the source to the 3D model of the rotor in the commercial software and compute it.
v. To compare the eddy currents computed from both 2D and 3D simulations
vi. To write a Master's Thesis based on all the computations, solutions and comparison made.

1.3 Outline of the Thesis

The background behind the thesis and the objectives of the project are discussed in Chapter 1. Chapter 2 highlights the finite element method and different numerical formulations used for the solution of eddy current problems. The step wise simulation process in the in-house software and its results are presented in Chapter 3. This chapter also presents the details about the design of the 3D model of the machine and also the simulations made in the commercial software. The results of the 3D simulation are also presented in the same chapter. Chapter 4 compares and draws conclusions from the simulation results and also presents possible potential areas of future research.

~ CHAPTER 2 ~

LITERATURE AND METHODOLOGY

Synopsis

This chapter deals with the brief introduction of different methods used for the solution of boundary value problems in electromagnetics, with special consideration to the numerical method using finite elements. A short introduction of a solid rotor induction motor is presented at the start. Different magnetic vector potential formulations used for the solution of eddy current problems are also discussed in this chapter. It also provides brief introduction to the methodology used in the project for solution of eddy current problems using finite element methods.

2.1 Solid rotor induction motor

Electrical machines work on the principle of energy conversion process through the electromagnetic field. From robotics to heavy load cranes, electrical machines have always played a vital role. There are various types of machine developed so far, which are categorized mainly with respect to their principle of operation and then their applications. Induction machines are one kind of electrical machines which are widely used in industrial drives and operate on the principle of electromagnetic induction. When the stator winding is energized with a supply, it creates a rotating magnetic field which then induces current in the rotor conductor. This current in turn interacts with the rotating magnetic field thus causing the rotation.

Solid rotor induction machine are special kind of induction machine in which the rotor is a solid body made of low-conductivity ferromagnetic alloy. It has the similar topology with the conventional induction machine with an exception in the rotor construction which may be smooth solid rotor as discussed by Brunelli et al.

(1983) or a solid rotor body slotted and embedded with copper bar as mentioned by Yang et al. (2008) or a solid rotor with slits as described by Aho et al. (2006). A solid rotor with a steel body is shown in Figure 2.1.

Figure 2.1 Smooth solid steel rotor. Kikuchi and Kenjo (1997)

In an induction machine, the rotor speed n is different from the rotating synchronous speed n_s of the stator flux. This speed difference is commonly referred to as the slip of the rotor and is often described as a fraction of the synchronous speed as follows

$$s = \frac{n_s - n}{n_s}$$

From the above relation, the frequency of the induced voltage in the rotor due to the relative motion of the stator flux and the rotor conductors can be deduced. The rotor speed from the above relation can be expressed as

$$n = (1 - s)n_s$$

The above relation can also be written in terms of angular velocity as

$$\omega_r = (1 - s)\omega_s$$

Now, in terms of frequency we have

$$f_r = sf_s$$

where, f_r is often called the slip frequency. Huppunen (2004) shows that the slip frequency and the angular speed of the rotor have a great significance as it not

only plays an important role in determining the penetration of magnetic flux in the rotor but act as a factor to determine the torque produced by the rotor.

The solid rotor shown in Figure 2.1 is a smooth solid rotor with a steel body. However, all solid rotors may not have a smooth body, as stated earlier. Ho et al. (2010), in their research have shown that the existence of axial slits in the solid rotor can cause the magnetic flux in the rotor to penetrate relatively deeper into the rotor and the analysis shows that having slits in the solid rotor will increase the torque of the machine by about 3.46 times than that of a rotor without slits. Welding a well-conducting non-magnetic material at the end faces of the rotor and equipping the solid rotor with a squirrel cage are two other possible ways to enhance the performance of the solid rotor, while sometimes the smooth solid-steel rotor may also be coated by a well conducting material for e.g. copper which have been shown by Huppunen (2004) in his Doctoral Thesis. Different schematic constructions of the solid rotor are shown in Figure 2.2.

Ho et al. (2010) also lists the advantages of the solid rotor induction machine as follows:

- Simplicity in its construction
- Low production cost and easy manufacturing
- High robustness against mechanical stress
- High thermal reliability
- High mechanical balance, stable

These merits are also supported by Gieras and Saari (2010) in their research paper and they also showed that these merits make solid rotor machine superior in applications that require high rotor strength, high critical speeds and good balancing properties.

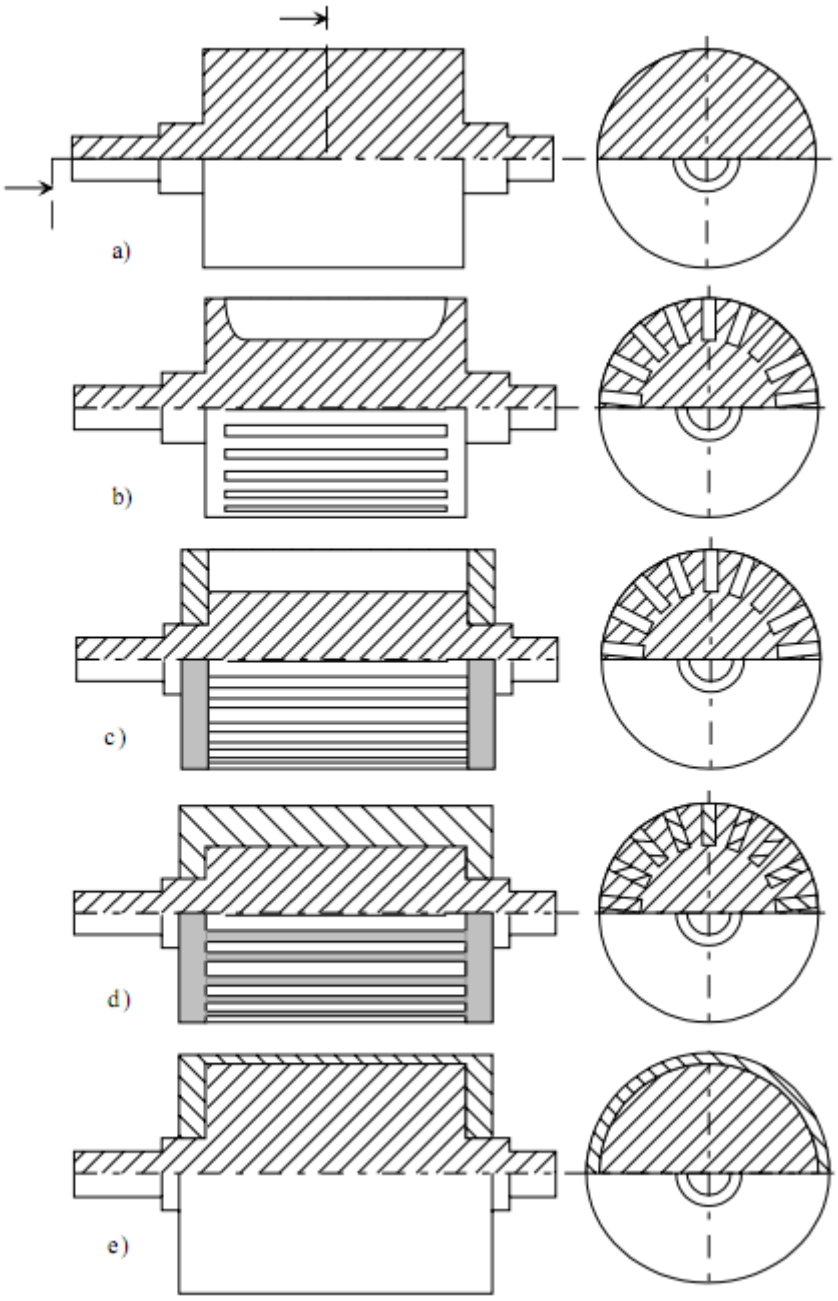

Figure 2.2 Solid Rotor Constructions: a) smooth solid rotor, b) slitted solid rotor, c) slitted solid rotor with end rings, d) squirrel-cage rotor, e) coated smooth solid rotor. Gieras (1995)

However, high rotor impedance and relatively low power density of the machine usually degrades its performance when compared with that of the conventional squirrel cage induction machine as stated by Ho et al. (2010). Gieras and Saari (2010) also say that the eddy current in the solid ferromagnetic rotor body is also responsible for the degradation of the machine's performance. Since, the solid

rotor is made up of a conducting material, with lower conductivity though, it sets a pathway for the magnetic flux as well as the induced eddy currents. This eddy current induced in the solid rotor tends to increase the losses, which may in turn lead to an increase of the temperature, thus degrading the performance of the machine. Therefore, eddy current loss and its distribution in the case of solid rotor machine has been a significant field of study with the aim to predict the machine performance and to find the ways to improve it.

2.2 Maxwell's Equations

Jackson (1999) in his book explains that the electric field and magnetic field can be considered to be almost independent when dealing with steady-state problems, but this independent nature no longer lasts when we consider a time-dependent problem. Time varying magnetic fields give rise to the electric fields and vice versa, which brings up a combined electrical and magnetic field term called electromagnetic. There are a set of equations that describe the fundamentals of electromagnetic fields and space and time relationship between electricity and magnetism. These equations are known as Maxwell's Equation. The differential form of Maxwell's Equation can be expressed as follows

$$\nabla . \boldsymbol{D} = \rho \qquad (1)$$

$$\nabla . \boldsymbol{B} = 0 \qquad (2)$$

$$\nabla \times \boldsymbol{E} = -\frac{\partial \boldsymbol{B}}{\partial t} \qquad (3)$$

$$\nabla \times \boldsymbol{H} = \boldsymbol{J} + \frac{\partial \boldsymbol{D}}{\partial t} \qquad (4)$$

where,

$\boldsymbol{E}$ is the electric field strength

$\boldsymbol{H}$ is the magnetic field strength

$\boldsymbol{D}$ is the electric flux density

$\boldsymbol{B}$ is the magnetic flux density

$\boldsymbol{J}$ is the electric current density

ρ is the electric charge density

The Maxwell Equations expressed above are simply the equations that describe four different laws in the field of electricity and magnetism. These different laws are more illustratively described when the Maxwell Equations are expressed in the integral form. The equations (1)-(4) can be expressed in the integral form by the use of the Gauss Theorem and the Stokes Theorem. Using Gauss Theorem on a volume *V* and its boundary surface *S*, the integral form of (1) and (2) can be obtained and expressed as

$$\oint \boldsymbol{D}.d\boldsymbol{S} = \oint \rho dV \qquad (5)$$

$$\oint \boldsymbol{B}.d\boldsymbol{S} = 0 \qquad (6)$$

Similarly using Stokes's Theorem and taking the integration over an open surface *S* and its boundary path *s*, we get the integral form for the equations (3) and (4) which can be expressed as

$$\oint \boldsymbol{E}.d\boldsymbol{s} = -\oint \frac{\partial \boldsymbol{B}}{\partial t}.d\boldsymbol{S} \qquad (7)$$

$$\oint \boldsymbol{H}.d\boldsymbol{S} = \oint \left(J + \frac{\partial D}{\partial t}\right).d\boldsymbol{S} \qquad (8)$$

Equations (5) and (6) describe the Gauss Law for Electricity and Magnetism respectively. Equation (5) relates the electric flux density with the total charge enclosed. It illustrates that the outflow of the electric flux density vector $\boldsymbol{D}$ over the closed surface S equals to the free electric charge enclosed within the surface. Similarly, equation (6) illustrates that the outflow of the magnetic flux density vector $\boldsymbol{B}$ vanishes. The Faraday's law of electromagnetic induction is described by the equation (7). It illustrates how the time varying magnetic field creates an electric field. Equation (8) generalizes the Ampere's circuital law with Maxwell's addition of displacement current $\frac{\partial \boldsymbol{D}}{\partial t}$. This equation is generally referred to as the Ampere's law with Maxwell's correction.

The variables in the equations above are related with each other by a set of constitutive relations that describes the different properties of the material and the

medium in which the material is placed. These constitutive relations can be expressed as

$$\boldsymbol{D} = \varepsilon \boldsymbol{E} \qquad (9)$$

$$\boldsymbol{B} = \mu \boldsymbol{H} \qquad (10)$$

$$\boldsymbol{J} = \sigma \boldsymbol{E} \qquad (11)$$

where, ε is the permittivity, μ is the permeability and σ is the conductivity of the material or medium in which the material is placed.

2.3 Finite Element Method (FEM)

Luomi (1993) presents his idea that electrical machines and other electromechanic devices operate on the principle of energy conversion through the electromagnetic field which makes their analysis to be done based on the solution of the field or on its approximation. Development of traditional calculation methods have been existed since long time, however, the recent development of computers and other numerical methods have made it quite convenient to deal with more complicated problems and moreover by solving the field equation directly. Finite Difference Methods (FDM), Boundary Element Method (BEM) and Finite Element Method (FEM) are some of the numerical methods used for solving the boundary value problems where a continuous problem is discretized and then its differential equation is solved by using a computer.

The main idea of Finite Element Analysis is to divide a large and complex problem area into small and simple problem areas. The small problem area is defined as an element. Then a solution is approximated in each small element using a function, generally a polynomial. This process of dividing a geometric model into small finite elements is called meshing. Figure 2.3 shows a first order finite element and Figure 2.4 shows the division of a circular geometry into small finite triangular elements.

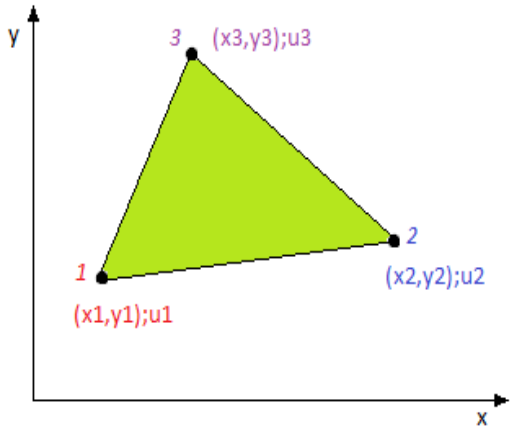

Figure 2.3 First order triangular element; (x_i,y_i) is the node coordinate and u_i is the value of potential at node i.

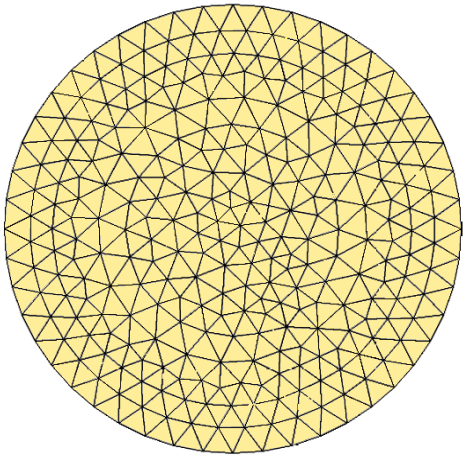

Figure 2.4 Triangular elements on a circular geometry

After creating a mesh, we define the sources and the boundary values of the problem. In each element, the solution (or potential) is approximated by using a polynomial which will give the matrix representation of each element. Approximation of the solution in each element by a polynomial will lead to an expression for the solution as

$$u(x,y) = \sum_{i=1}^{n} \mathrm{N_i}\,(x,y)u_i \qquad (12)$$

Where, $N_i(x,y)$ is called the global shape function and is non-zero only in those elements to which node *i* belongs to and *n* is the total number of nodes in the problem region.

Combination of all elemental matrices will lead to the global system matrix. Then we apply all the necessary boundary conditions and solve the resulting equations to get the result.

Kanerva (2001) presents Finite Element Analysis as a powerful tool for the analysis of magnetic fields in electrical machines and the electrical state of different components of machine can also be derived based on that solution. However, for proper analysis, both the magnetic field equation and the circuit equation should be used in conjunction with each other, i.e. they must be coupled.

2.4 Eddy Current Formulations

In any electromechanical device accounting the time variation of magnetic field, the variation of magnetic field with time will induce an electric field which in turn will cause a current to flow in the conducting medium of the device. This current is called eddy current. The induced eddy currents again tend to affect the magnetic field. This is the reason why we need to solve both electric and magnetic field equations together to solve the eddy current problems.

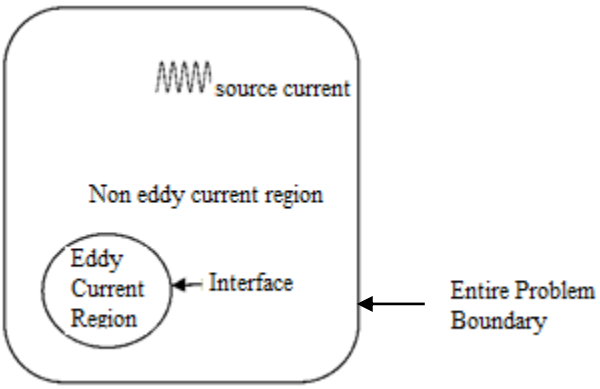

Figure 2.5 Eddy current problem

A typical eddy current problem consists of an eddy current region with a finite conductivity surrounded by a non-conducting eddy current free region which however may contain the source currents as depicted in Figure 2.5. The boundary of the eddy current region is the interface between the conducting and the non-conducting regions.

According to Luomi (1993), in general case, there are two basic formulations used for the solution of eddy current problems and they are $\boldsymbol{A} - \phi$ formulation and $\boldsymbol{T} - \Omega$ formulation. However, literature shows that there are several others formulations derived recently mainly for the 3-D problems. The $\boldsymbol{A} - \phi$ formulation uses the magnetic vector potential $\boldsymbol{A}$ and the reduced scalar potential ϕ to solve the eddy current problems. The differential equation obtained from this type of formulation is

$$\nabla \times (\upsilon \nabla \times \boldsymbol{A}) + \sigma \frac{\partial \boldsymbol{A}}{\partial t} + \sigma \nabla \phi = \boldsymbol{J}_s \qquad (13)$$

Where, υ is the reluctivity of the material, σ is the conductivity of the medium and $\boldsymbol{J}_s$ is the current density of the source. The differential equation above is derived from the Maxwell's Equations and the definition of magnetic vector potential,

$$\boldsymbol{B} = \nabla \times \boldsymbol{A} \qquad (14)$$

Substituting (14) in the Maxwell's equation $\nabla . \boldsymbol{B} = 0$, and again substituting the resulting equation to $\nabla \times \boldsymbol{H} = \boldsymbol{J}$, we obtain the partial differential equation

$$\nabla \times (\upsilon \nabla \times \boldsymbol{A}) = \boldsymbol{J} \qquad (15)$$

We already know that the change in magnetic field induces an electric field which in turn produces the eddy current. From Maxwell's equation $\nabla \times \boldsymbol{E} = -\frac{\partial \boldsymbol{B}}{\partial t}$ and (14) we obtain $\nabla \times \boldsymbol{E} = -\nabla \times \frac{\partial \boldsymbol{A}}{\partial t}$, so that the electric field strength $\boldsymbol{E}$ is given by,

$$\boldsymbol{E} = -\frac{\partial \boldsymbol{A}}{\partial t} - \nabla \phi \qquad (16)$$

Since, the current density $\boldsymbol{J} = \sigma \boldsymbol{E}$, from (15) and (16) we have

$$\nabla \times (\upsilon \nabla \times \boldsymbol{A}) = -\sigma \frac{\partial \boldsymbol{A}}{\partial t} - \sigma \nabla \phi \qquad (17)$$

The current density corresponding to (17) is the eddy current density as it is produced by the electric field which is induced by the change in the magnetic field, so (17) is valid for eddy current regions. But, the current density corresponding to (15) is the source current density that is the current density in the source coils and windings. So, both equations (15) and (17) are combined to give a single equation which corresponds to the whole problem region which is expressed as given in (13).

The divergence of the eddy current density vanishes, which gives us another equation

$$\nabla.\left(\sigma\frac{\partial \boldsymbol{A}}{\partial t}+\sigma\nabla\phi\right)=0 \qquad (18)$$

The tangential component for the electric field $\boldsymbol{E}$ and the normal component of $\sigma\frac{\partial \boldsymbol{A}}{\partial t}+\sigma\nabla\phi$ is continuous at the interface between the eddy current region and non-eddy current region.

The electric vector potential $\boldsymbol{T}$ and the magnetic scalar potential Ω are used to derive the $\boldsymbol{T}-\Omega$ formulation, where $\boldsymbol{T}$ is defined such that $\nabla.\boldsymbol{T}=0$. Also, the magnetic field strength is defined as $\boldsymbol{H}=\boldsymbol{T}-\nabla\Omega$. From this definition of magnetic field strength and Maxwell's equation $\nabla\times\boldsymbol{H}=\boldsymbol{J}$, we find that the curl of the electric vector potential is equal to the current density, that is $\nabla\times\boldsymbol{T}=\boldsymbol{J}$.

Now, the electric field $\boldsymbol{E}$ can be written as $\boldsymbol{E}=\frac{\boldsymbol{J}}{\sigma}=\frac{\nabla\times\boldsymbol{T}}{\sigma}$ and the magnetic flux density $\boldsymbol{B}$ can also be written as $\boldsymbol{B}=\mu\boldsymbol{H}=\mu(\boldsymbol{T}-\nabla\Omega)$. Substituting the expression of $\boldsymbol{E}$ and $\boldsymbol{B}$ in Maxwell's equation $\nabla\times\boldsymbol{E}=-\frac{\partial \boldsymbol{B}}{\partial t}$, we obtain

$$\nabla\times\left(\frac{\nabla\times\boldsymbol{T}}{\sigma}\right)=-\frac{\partial}{\partial t}[\mu(\boldsymbol{T}-\nabla\Omega)] \qquad (19)$$

Substituting the expression for $\boldsymbol{B}$ in Maxwell's equation $\nabla.\boldsymbol{B}=0$, we obtain another equation

$$\nabla.\mu(\boldsymbol{T}-\nabla\Omega)=0 \qquad (20)$$

In $\boldsymbol{T}-\Omega$ formulation, the tangential component of the magnetic field strength $\boldsymbol{H}$ must be continuous which makes the electric vector potential $\boldsymbol{T}$ continuous at the

interface. Also the normal component of $\mu(\boldsymbol{T} - \nabla\Omega)$ is continuous at the interface.

In two dimensional eddy current problems, the magnetic vector potential, the electric field strength and the current density are all *z*-directed and the field is calculated in the *xy*-plane. The gradient $\nabla\phi$ is also *z*-directed and moreover the assumption that there is no existence of potential differences due to the electric charge (since the conductivity is assumed to be constant in the conducting region) makes ϕ equal to zero. Thus the partial differential equation for the computation of 2-D eddy current problems becomes

$$\nabla \times (\upsilon\nabla \times \boldsymbol{A}) + \sigma\frac{\partial \boldsymbol{A}}{\partial t} = \boldsymbol{J}_s \qquad (21)$$

Now, this PDE is discretized to get a system of ordinary differential equation, which is then solved by various methods like Euler Methods, Runge-Kutta Method, Crank-Nicholson Method, Gear Method, Newton Method etc.

The three dimensional computation of eddy current fields has been the subject of extensive research for the international community of numerical analysts. Their dedicated to work on the investigation of electromagnetic field from early 80's which can be well understood by the number of scientific contributions in this field seen at that time, for instance in Biro and Preis (1989). Various formulations have been developed, generally based on the $\boldsymbol{A} - \phi$ formulation or $\boldsymbol{T} - \Omega$ formulations. $\boldsymbol{A}, \phi - \boldsymbol{A}$ formulation, $\boldsymbol{A}, \phi - \psi$ formulation, $\boldsymbol{A}, \phi - A - \psi$ formulation are some examples of the formulations using magnetic vector potential, reduced electric scalar potential and electric scalar potential. However, the solution of large systems of equations leads to increased number of unknowns which cause unreasonably high computation time and cost and 3-D calculations of eddy current become very difficult which is also explained by Muller and Knoblauch (1985) in their research. Various researches have been carried out to overcome these difficulties.

In 3-D eddy current problems, both the electric and the magnetic field must be described in the conductors while in the regions which are free from eddy currents, only magnetic field needs be accounted for as presented by Biro and Preis (1990). Biro and Preis (1990) also suggests that different sets of potentials may be used in conducting and eddy current free regions but it may cause problems while interfacing them on the conductor surface. Many formulations for 3-D eddy current problems have been developed in order to solve this problem. $A, \phi - A$ formulation is obtained when the potentials A, ϕ in conductors are coupled with A outside the conductors. Similarly when the potentials T, ψ in the conductors are coupled with the ψ in the eddy current-free regions, $T, \psi - \psi$ formulation is obtained. Balchin and Davidson (1983) found out that advantages of using the magnetic scalar potential in the non-conducting domain and suggested that the use of ψ in the non-conductor region instead of A in the $A, \phi - A$ formulation, the problem of $A, \phi - A$ having large number of unknowns in the eddy current-free regions can be minimized and this gave the $A, \phi - \psi$ formulation. Though $A, \phi - \psi$ formulation overcomes the difficulties of the $A, \phi - A$ formulation, it is still unable to treat multiply connected conductors which is also explained by Biro and Preis (1990). The problem of multiply connected conductors can be possibly addressed through the method suggested by Leonard and Rodger (1988) by using A instead of ψ in the non-conducting holes of the conductors in the multiply connected conductors, which gives the $A, \phi - A - \psi$ formulation.

2.5 Time-Stepping Analysis

The finite element analysis of an electrical machine, when only the sinusoidal supply is considered is regarded as Time-Harmonic Analysis (THA). The computational time in THA is quite short. But it does not consider some higher harmonics and also the motion of the rotor is not accounted for. Therefore, Time-Stepping Analysis (TSA) method is used in order to consider both the motion of the rotor and the harmonics related to it. In this case, the circuit equations are also solved together with the field equations. To consider the motion of the rotor, the

elements in the air gap are modified at each time step during the discretization of the field equation as presented by Davat, Ren and Lajoie-Mazenc (1985). This method of modeling the movement of the rotor in a machine model has also been used and discussed by Arkkio (1990).

The partial differential equation (21) can be discretized to get a system of ordinary differential equations, which can be then solved by different methods like Euler Methods, Runge-Kutta Method, Crank-Nicolson Method, Gear Method, Newton Method etc. However, a generalized first-order finite difference procedure can be used to get a solution by time stepping. If, at time step t_{k-1}, the nodal value is $\mathbf{a_{k-1}}$ then at time step t_k, the nodal value $\mathbf{a_k}$ is given by

$$\mathbf{a_k} = \mathbf{a_{k-1}} + \left[\beta \frac{\partial \mathbf{a}}{\partial t}\bigg|_k + (1-\beta)\frac{\partial \mathbf{a}}{\partial t}\bigg|_{k-1}\right]\Delta t$$

where, Δt is the length of the time step; β is a weighting parameter between 0 and 1, the most popular values used for β being 0 for Direct Euler Method, 0.5 for Crank-Nicolson (trapezoidal) method and 1for backward Euler method. These values of β for the discretization process have also been used by Islam and Arkkio (2008).

2.5 Methodology

This project mainly deals with the investigation of the solution of problems related to the coupled field in electrical machine with different dimensions. The investigation of a coupled 2D-3D model of solid rotor of a high speed induction machine is the main agenda of the project where eddy current computation and analysis is the primary interest.

After studying relevant literatures and gathering information and knowledge about the background and literatures related to the project, the initial work was started which consisted of computing the magnetic vector potential or magnetic flux density in a two-dimensional model of the machine. For this purpose, an in-house 2D finite element software FSCMEK was used. A three-phase, 50 Hz, 380 V, star connected, 7.5 kW solid rotor induction machine was considered. The rotor of the

machine is made up of a steel body with slits. The 2D model of the machine was simulated. The solution obtained from this computation was to be used as a source for the 3D model of the rotor. Since the in-house software FCSMEK was limited to the 2D modeling only, the 3D modeling and computations were done using commercial finite element software called COMSOL Multiphysics™. The 3D CAD-model of the machine was constructed in SolidWorks™ and then imported to the COMSOL Multiphysics™. The parameters of the model used for 3D simulation were the same as these used in FCSMEK. After having obtained the solution from 2-D simulation, the resulting nodal values of magnetic vector potential were tried to use as a source in the 3-D model. Matlab was used for data transfer between FCSMEK and COMSOL Multiphysics™. However, the task of transferring the nodal values of the magnetic vector potential was very tedious. So, an alternative way was chosen, that is using the current density in the stator slots computed from FCSMEK as a source in the slots of the model in the 3-D model. The 3D model was then simulated and then the eddy current loss was calculated. This eddy current loss was compared with the one obtained from the 2D solution in FCSMEK.

~ CHAPTER 3 ~

FEM MODELS AND SIMULATIONS

Synopsis

This chapter deals with the details of all the simulations carried out during the study. Firstly, it describes the 2D simulations performed in the in-house software and its results. The construction of both the physical and the finite element 3-D model is also well described in this chapter. All the definitions and assumptions made for the modeling are included here.

3.1 Machine Parameters

This study deals with the investigation of eddy current loss calculation in solid steel rotor of an induction machine. Both 2-D and 3-D models of the machine are taken into account and computation based on finite element method is carried out. The machine under study is considered to be a three phase, 50 Hz, 380 V, star connected, 7.5 kW solid steel rotor induction machine. The cross-section of the machine under study is shown in Figure 3.1 and the machine parameters are listed in Table 3.1.

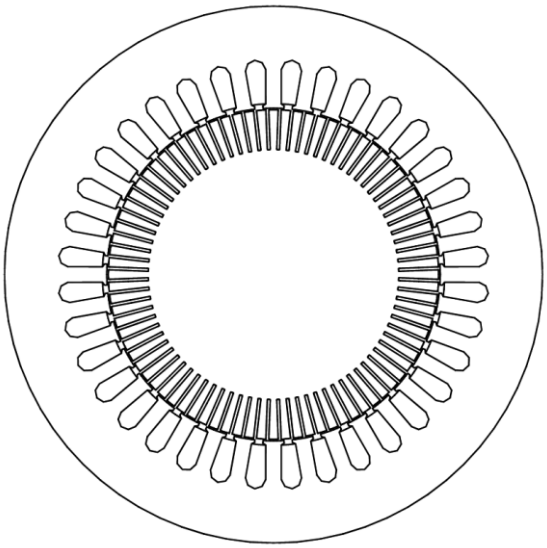

Figure 3.1 2-D cross-section of the machine under study

Table 3.1 Machine Parameters

Parameter	Value
Rated power [kW]	7.5
Rated voltage [V]	380
Rated frequency [Hz]	50
Rated slip	0.05
Number of poles	4
Number of phases	3
Number of parallel paths	1
Number of conductors in a stator slot	20
Coil pitch in slot pitches	9
Effective length of the machine [m]	0.146
Outer diameter of the stator core [m]	0.202
Inner diameter of the stator core [m]	0.125
Number of stator slots	36
Outer diameter of the rotor core [m]	0.124
Inner diameter of the rotor core [m]	0.047
Number of rotor slots	84
Resistance of a stator phase at 20°C [Ohm]	0.527
End-winding reactance of a stator phase [Ohm]	0.239

The stator core is made up of a magnetically non-linear material called Electrical steel sheet – Bochum STABOLEC 260-50 A. The stator core is assumed to have zero electrical conductivity. The rotor core material is also a magnetically non-linear ferromagnetic material made up of Construction Steel (Ovako 520 L). The solid rotor has a finite electrical conductivity of $4.30 \times 10^6\ S/m$. The solid rotor has 84 axial slits which is advantageous in terms of the torque of the machine. The stator has 36 slots for the stator winding. The winding material is copper, the conductivity of which is set to $58.1 \times 10^6\ S/m$.

3.2 2D Finite Element Simulation in FCSMEK

The initial step of the investigation was to perform a finite element analysis of the 2 dimensional model of the given machine. For this purpose, the in-house finite element software FCSMEK was used. The software has a collection of programs and routines designed for the finite element analysis of synchronous and asynchronous radial flux machines.

The machine parameters mentioned in Table 3.1 among others were given as an input file to the software. The software creates geometry from the parameters in the input file. The equations to be solved are also defined in the program of the software. The basic governing equation of electromagnetism defined in the equation (13) is solved along with the circuit equations of the machine. The non-linearity of the stator and the rotor materials are defined by the non-linear BH-Curve for each material. The BH-Curve for the stator and the rotor materials are shown in Figure 3.2 and Figure 3.3 respectively.

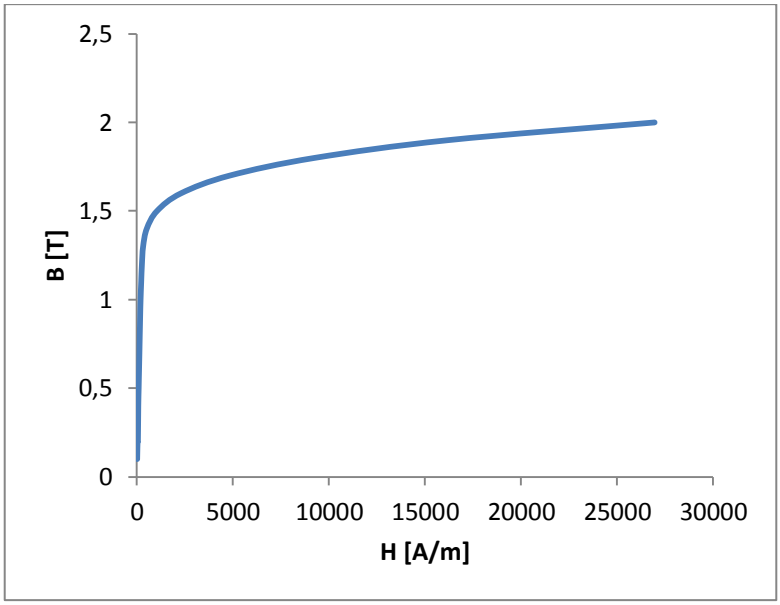

Figure 3.2 BH Curve of the stator core material

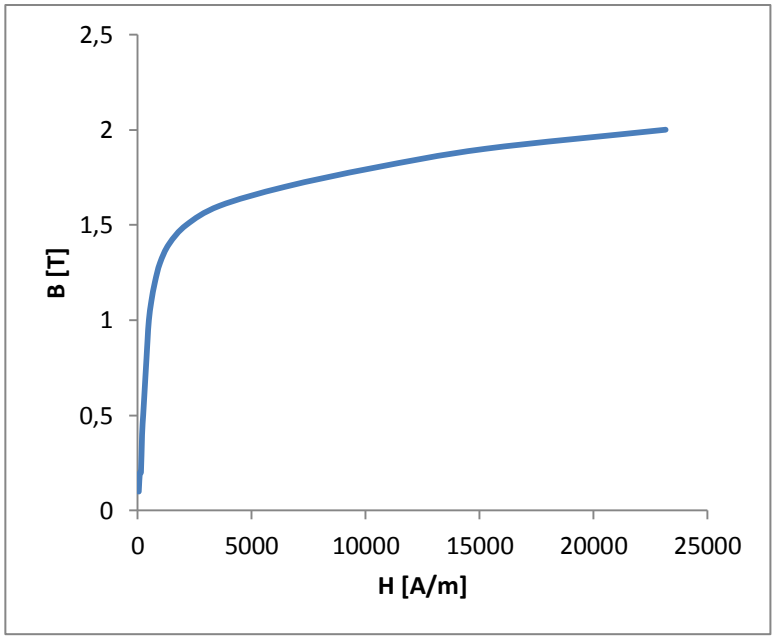

Figure 3.3 BH Curve of the rotor core material

A time-stepping finite element analysis is performed on the model .The Crank-Nicolson method is used for time-stepping study. However, if the time-stepping is started from a zero field, the computational time becomes extensively high due to the large time constants associated with the inductances of the windings. Therefore, to avoid such large computational time, a time harmonic solution is performed, the solution of which is used to calculate the initial value for the time-stepping analysis. The motion of the rotor is modeled by creating a changeable finite element mesh in the air-gap of the machine. The mesh is divided into two parts. The upper part contains the stator and the air gap and the lower part contains the rotor. The nodes on the rotor surface and the air gap surface are connected with a periodic boundary condition. The rotation is achieved by changing the form of the element in the air gap at each time step.

The basic steps for the study of the given machine using finite element method in the in-house software FCSMEK can be represented by a simple flowchart shown in Figure 3.4. The ‘bold’ terms in the parenthesis in the process box of the flowchart are the name of the program in FCSMEK.

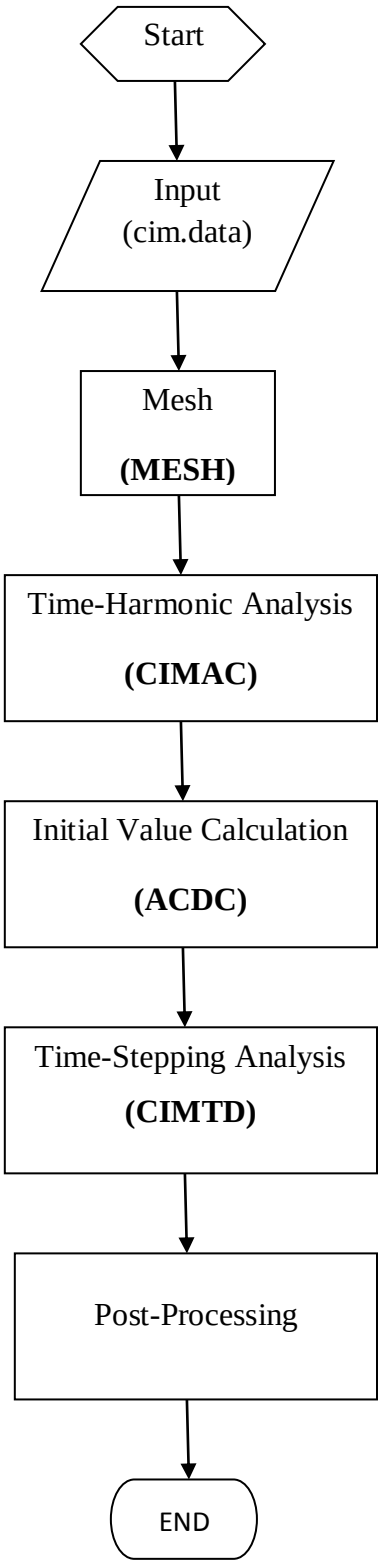

Figure 3.4 Flow Chart of Finite Element Simulation steps used in FCSMEK for 2D study

3.3 Results from FCSMEK

Four periods of line frequency were simulated with 400 times steps per period of line frequency. The total computational time was 260 seconds. Initially, the **MESH** program generates a finite element mesh for the cross-sectional geometry of the machine based on the data from the input file which contains the necessary dimensions, slot numbers and slot indices. The program creates the smallest possible symmetrical sector of the cross-section of the machine and draws the triangular elements in it. A first order, changeable finite element mesh was made in order to consider the rotation of the rotor, which is already explained in the previous section. The resulting mesh consisted of 4032 elements and 2044 nodes. There were 396 elements and 248 nodes in the stator and 3354 elements and 1796 nodes in the rotor. The air gap of the machine consisted of 282 finite elements. The resulting mesh is shown in Figure 3.5.

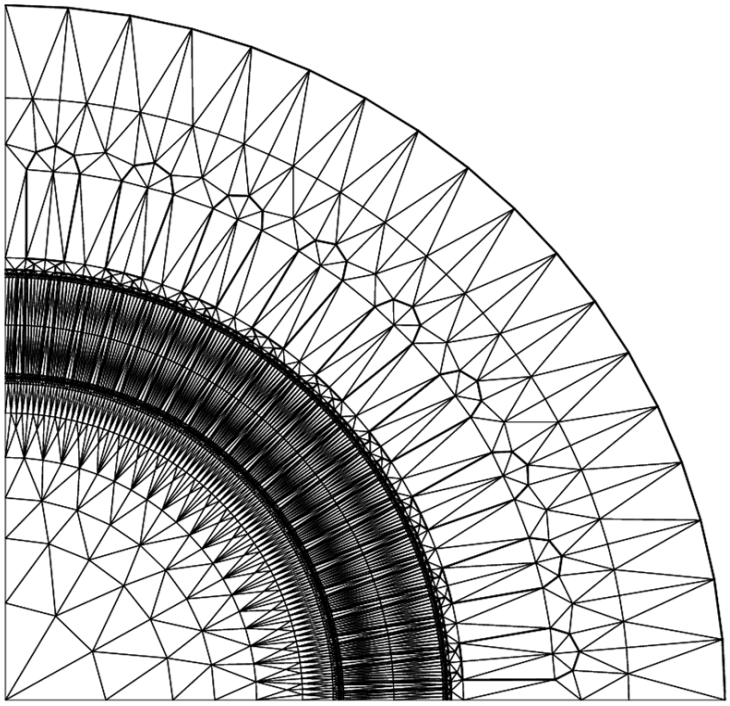

Figure 3.5 Finite element mesh in the symmetric cross-section using FCSMEK

After creating the mesh in the two-dimensional geometry of the given machine, the time-harmonic simulation was performed. The program uses Newton-Raphson method to solve the non-linear system of equations obtained by the finite element

method. The results obtained from the time-harmonic analysis are shown in Table 3.2.

Table 3.2 Operating Characteristic of the machine obtained from the Time-Harmonic Analysis

Parameter	Value
Terminal voltage [V]	380
Supply frequency [Hz]	50
Line current [A]	14.98
Power factor	0.695
Slip [%]	5
Torque [Nm]	40.291
Rotation speed [rpm]	1425
Input Power [kW]	6.584
Shaft Power [kW]	6.095
Resistive stator loss [W]	438.2
Resistive rotor loss [W]	320.8
Core loss [W]	134.2

The magnetic flux density distribution resulting from the time stepping analysis of the three-phase, 50 Hz, 380 V, star connected solid rotor induction machine at 5% slip is shown in the Figure 3.6. The figure shows the magnetic flux distribution in whole cross-section of the machine. The contours throughout the cross-section in the Figure 3.6 are the equipotential lines. We can see that flux lines make a spiral shape in the rotor. This can be because of the magnetic field produced by the induced eddy currents in the rotor, which are circulating and produce a magnetic field which are circulating around the path of the current. The characteristics of the machine obtained from the time-stepping analysis are tabulated in Table 3.3.

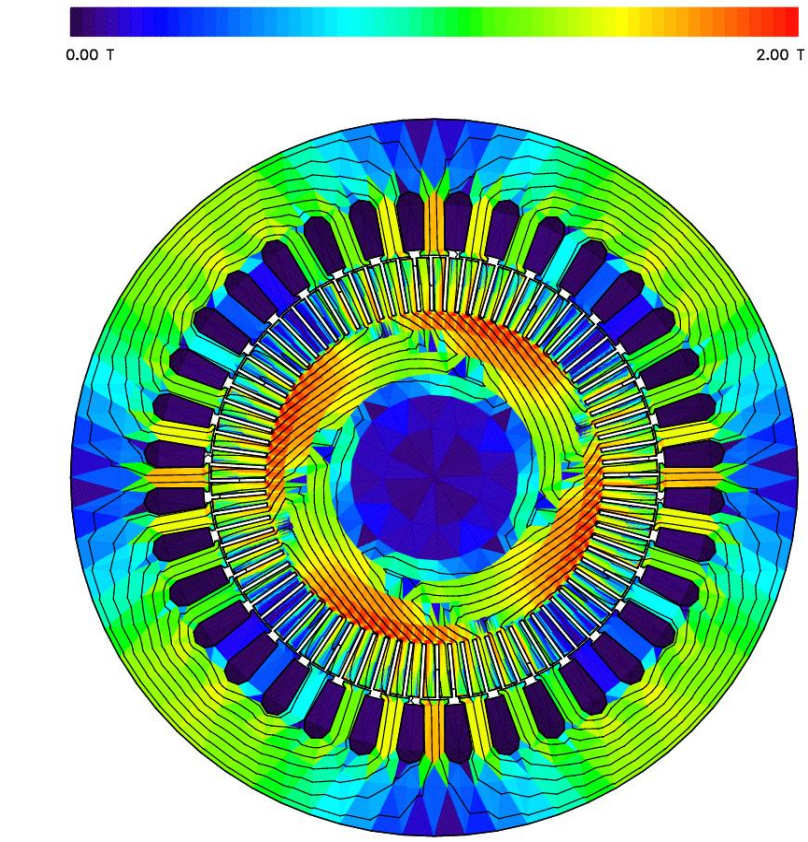

Figure 3.6 Computed magnetic flux density distribution in the cross section of the machine. Time Harmonic Analysis.

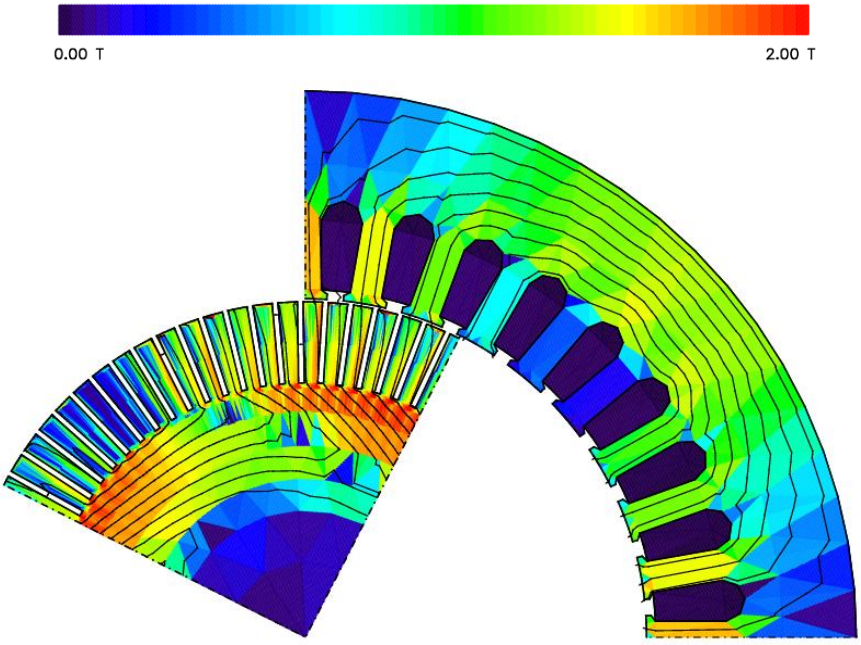

Figure 3.7 Computed magnetic flux density distribution in the computed region along with the motion of the rotor shown. Time Stepping Analysis.

Table 3.3 Machine Characteristics resulting from TSA

Parameters	Value
Terminal voltage [V]	380
Supply frequency [Hz]	50
Slip [%]	5
Terminal current [A]	14.665
Peak current [A]	20.710
Power factor	0.7165
Rotational speed [rpm]	1425
Air-gap torque [Nm]	35.445
Input Power [kW]	6.92
Shaft power [kW]	5.29
Air-gap flux density [T]	0.877
Current density in a stator slot [A/mm^2]	2.88
Resistive stator loss [W]	420.04
Resistive rotor loss [W]	1173.52
Core loss in stator [W]	130.51
Core loss in rotor [W]	76.57
Total stator loss [W]	550.67
Total rotor loss [W]	1249.80
Total electromagnetic loss [W]	1800.48

Figure 3.6 shows the magnetic flux distribution in whole cross-section of the machine. However, to reduce the computational time, only one symmetric sector of the cross-section of the machine is taken into account for simulation. The magnetic flux distribution in the region which is taken into account for computation is shown in Figure 3.7. The motion of the rotor can also be understood from this figure.

The three-phase current in the stator winding resulting from the simulation is shown in Figure 3.8. The current density in the stator slot is used as a source in the simulation carried out in the commercial software.

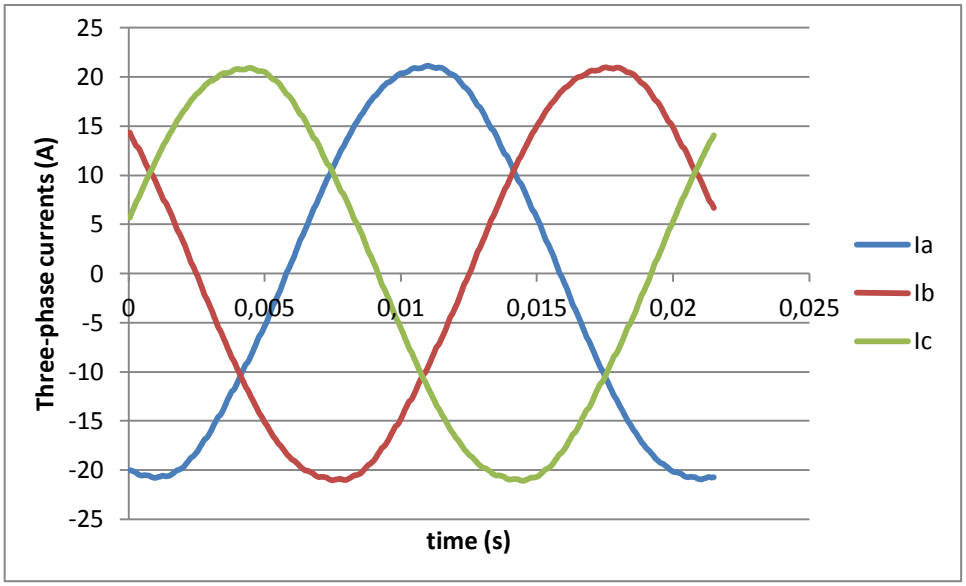

Figure 3.8 Three-phase current in the stator winding computed by the TSA.

The fundamental air gap flux density resulting from the time-stepping analysis is 0.87 Tesla, which is reasonable for an induction machine. The calculated average air gap torque is equal to 35.45 Nm and the time variation of the torque is shown in Figure 3.9. Only one periods of the line frequency is considered.

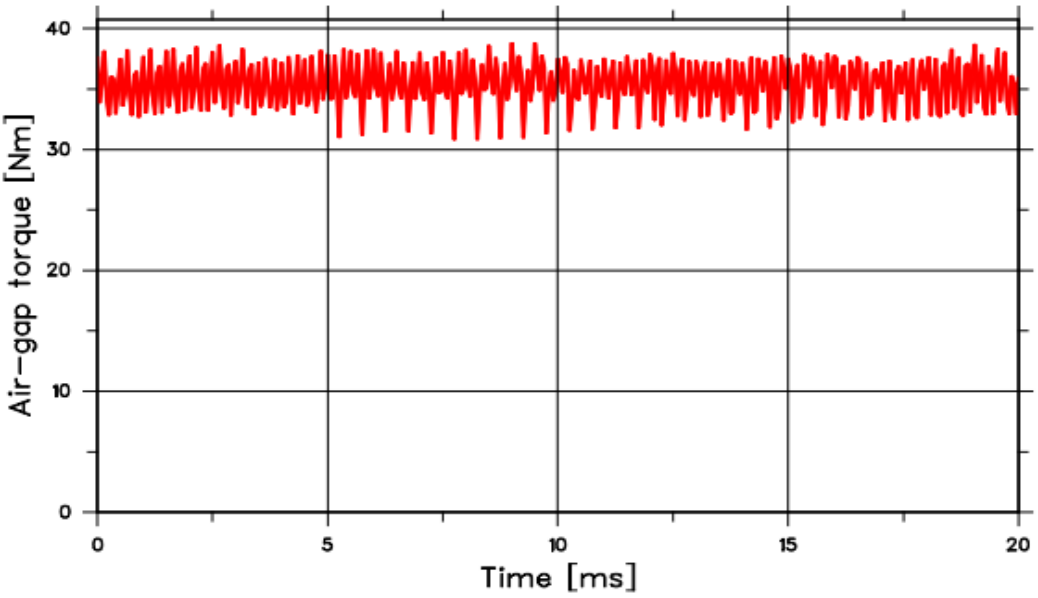

Figure 3.9 Time variation of Torque computed with the TSA.

The losses in the machine mainly include the total core loss as well as the total resistive losses in both stator and the rotor. The total loss calculated from the study is equal to 1.8 kW. The resistive loss in the stator is the I^2R loss in the

winding of the stator slot which is due to the flow of source current. However, the given machine under study being a solid rotor machine does not consist of conductor windings in the rotor. Therefore, the resistive loss that occurs in the rotor is due to the currents that are induced in the rotor body. The conductivity of the solid steel is involved. These induced currents are the eddy currents and the losses due to these currents are the eddy current losses in the rotor of the machine. These losses can be determined by integrating the term $\boldsymbol{J}^2/_{\sigma}$ over the volume of the rotor, where $\boldsymbol{J}$ is the eddy current density in the rotor and σ is the conductivity of steel. The calculated resistive loss in the rotor is around 1.173 kW and the loss distribution is shown in Figure 3.10.

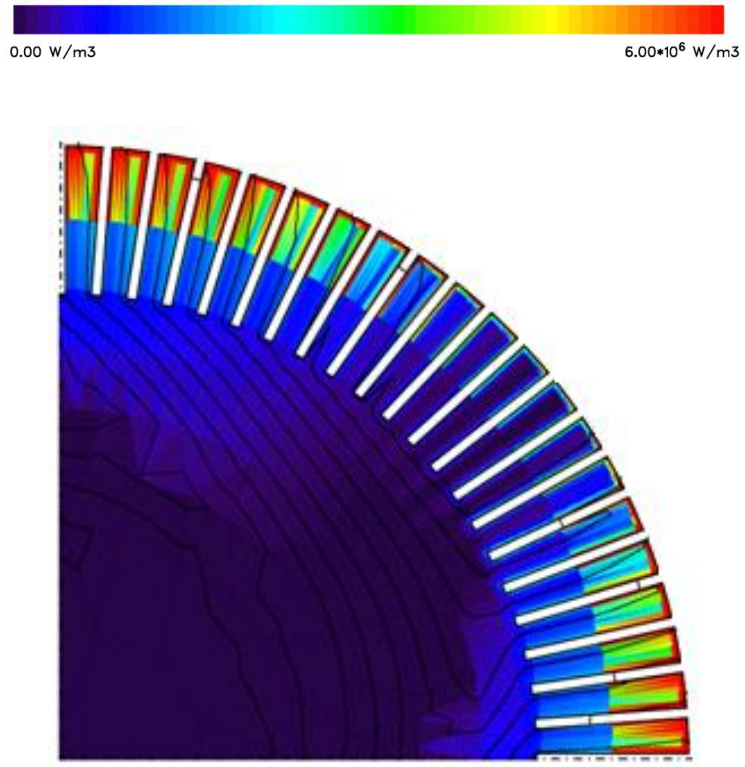

Figure 3.10 Eddy Current loss distribution in the rotor.

It can be seen from Figure 3.10 that the eddy currents have larger values towards the surface of the rotor than the core which may emphasize the small skin depth in the rotor. The eddy currents are mainly distributed at the surface of the rotor teeth.

3.4 3-D Physical Model

For the 2-D analysis in FCSMEK, the geometry was already defined in the software through parameterization of different slot shapes. The geometrical parameters of the two dimensional cross-section of the machine was defined in the input file, according to which the program in the software created the mesh in the geometry. The 2-D geometry of the machine is shown in Figure 3.1.

As stated earlier, due to the limitation of the in-house software FCSMEK, the 3-D computation and analysis was performed in commercially available software. However, the commercially available software did not have any pre-defined machine geometry on which the study could be done. So, a 3-D geometrical model of the machine had to be constructed. Since, this study dealt with the finite element analysis in different dimensions of the same machine, each and every geometrical dimension used for the construction of the 3-D model had to be equal to the ones defined in the machine parameters of the in-house software FCSMEK used for the 2-D simulation. This will not only assure for the different dimensions of the same machine to be considered but also accounts for the reasonable accuracy of the simulated results.

The 3-D model of the solid steel rotor induction machine used in the project was constructed by using SolidWorks™ which is commercially available CAD software. The length of the machine, inner and outer diameters of the stator and the rotor, and the number of slots in the stator and rotor are given in Table 3.1. The same parameters are used for designing the 3-D geometry.

To obtain a reasonable accuracy in the computation results in both simulations, the design dimensions of each part of the geometry had to be specially considered. There are 36 slots in the stator and the type of slot built was the same as that of the geometry used in FCSMEK, which is shown in Figure 3.11. The dimensions of various sections of the stator slot are listed in Table 3.4.

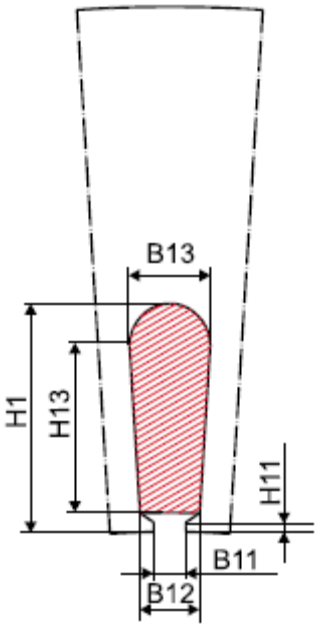

Figure 3.11 Shape and dimension parameters of the stator slot.

Table 3.4 Dimensions of different sections of stator slot

Parameter	Value
H1 [m]	0.0183
H11[m]	0.001
H13 [m]	0.0123
B11 [m]	0.003
B12 [m]	0.0053
B13 [m]	0.0075

The machine under study is an induction machine with a solid rotor. However, to improve the torque in high speed application the solid rotor often consists of axial slits as shown by Ho et al. (2010). The rotor slit used in the geometry is shown in Figure 3.12 and the dimension of various section of the rotor slit is listed in Table 3.5

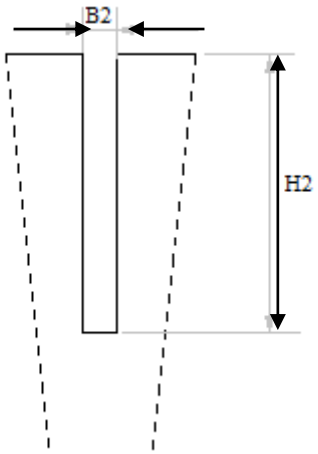

Figure 3.12 Rotor Slit

Table 3.5 Dimensions of different sections of rotor slit

Parameter	Value
H2 [m]	0.015
B2 [m]	0.001

With the above discussed geometrical parameters, their design and dimensions, the 2-D cross-section of the machine was constructed and then extruded to obtain a 3-D geometry which, was later used for the three dimensional finite element analysis in COMSOL Multiphysics™. The 2-D and 3-D geometry are shown in Figure 3.13 and Figure 3.14 respectively.

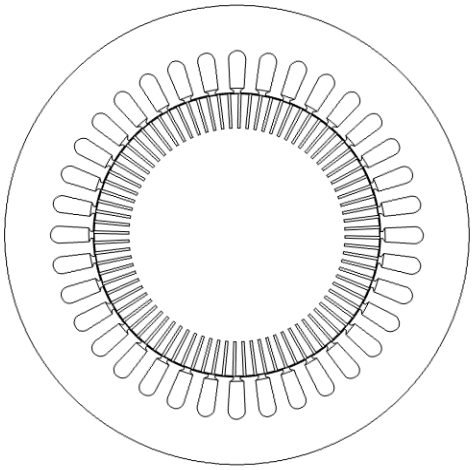

Figure 3.13 2-D cross-section of machine built in SolidWorks™

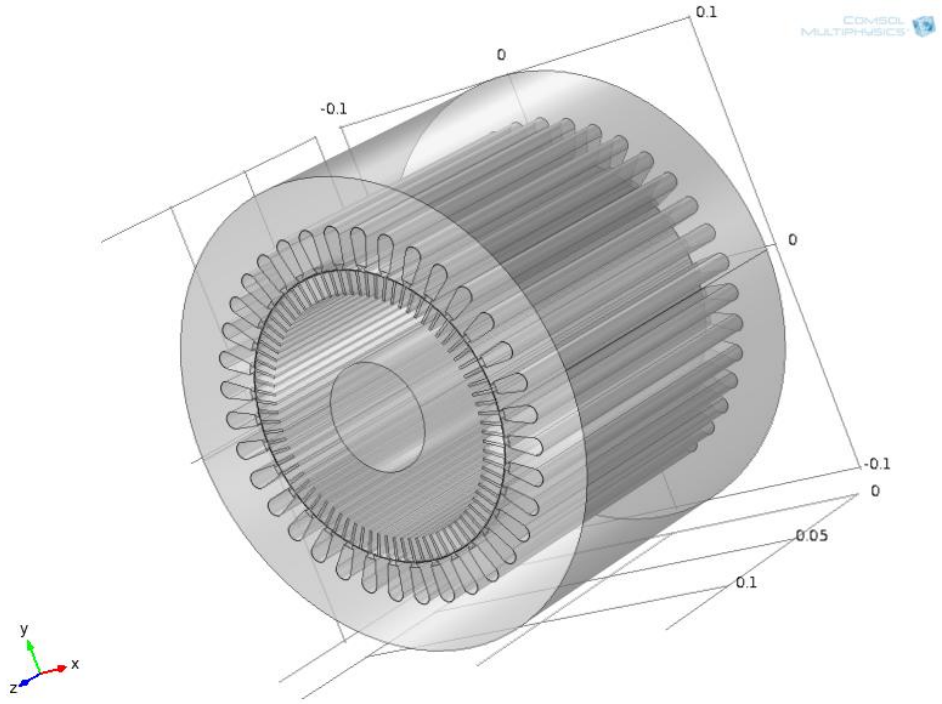

Figure 3.14 The 3-D geometrical model

3.5 Data Transfer

In this thesis, we tried to use the solution obtained from FCSMEK as a source to the simulation in COMSOL Multiphysics™. The main idea behind this was to realize a coupled electromechanical model of the machine under study, in which the 2D model of the machine was coupled with the 3D model of the rotor. For this, the magnetic vector potential was used as the transferred variable. Our own Matlab codes and subroutines were used for the entire data transfer process. FCSMEK calculates the magnetic vector potential for each node in the mesh and stores them along with other mesh information in a file called *cim.fedat*. A Matlab code was used to read the file *cim.fedat* from FCSMEK to Matlab and store the nodal values of the magnetic vector potential along with the node coordinates that was stored in a database. Our idea was to run a 2D simulation of the same machine and under same condition, and then read the mesh file from COMSOL Multiphysics™ and then replace the coordinates of the nodal point and the corresponding nodal values of the vector potential by those from FCSMEK. The

2D simulation in COMSOL Multiphysics™ is described later in this report. A different routine was used to import the COMSOL Multiphysics™ mesh into Matlab. The nodal coordinates and the nodal values of the magnetic vector potential obtained from COMSOL Multiphysics™ were then replaced by those obtained from FCSMEK manually. The modified mesh was then imported to COMSOL Multiphysics™ again but the modified mesh was not supported due to which the desired coupled model was not obtained. Moreover, the replacement of the nodal coordinates and the corresponding nodal values of the vector potential in the COMSOL Multiphysics™ mesh manually to modify the mesh was tedious and time consuming. Therefore, this process of data transfer was regarded as inappropriate.

Another method of data transfer used during the study was quite simple and successful. This included a different variable than the previous one. In this case, the current density in the conductors in the stator slot was used as the variable to be transferred. At first, the file called *cimtd.tulos*, that contained the solution of the time-stepping finite element analysis in FCSMEK, was read in Matlab by using our own routine. The time-stepped values of three-phase current density in the windings of the stator were read from the file with the help of the MATLAB routine. These values of the three-phase current density were stored in a database. Later these current densities were used as an external current density source in the model studied in COMSOL Multiphysics™.

All Matlab codes and routines used for the data transfer process are shown in the APPENDIX A and APPENDIX B.

3.6 Simulation in Comsol

3.6.1 2D Model

Thanks to the present day computing resources, the FEM analysis of magnetic fields in a complicated geometry has become possible. The two dimensional finite element analysis of the given solid rotor induction machine has already been performed in the in-house software FCSMEK and the results have been

thoroughly analyzed. However, as an initial approach to use the commercially available software, the two dimensional study of the machine was again performed in COMSOL Multiphysics™.

The Maxwell equations and other governing equations for the calculation of eddy currents have already been discussed in the previous chapter. The $\boldsymbol{A}-\phi$ formulation was used for the two dimensional finite element calculations of the eddy currents. The governing equation for $\boldsymbol{A}-\phi$ formulation of the eddy currents used in this study is given in Equation (13).

This equation is solved only in the conduction region that is the region where the eddy currents are present. But in the non-conducting region that is the region free of eddy currents, the eddy current density given by $\sigma\frac{\boldsymbol{\partial A}}{\boldsymbol{\partial t}}+\sigma\nabla\phi$ is assumed to be zero. However, it is assumed that such region may include the current density due to the source current. Thus the equation solved for non-eddy current region is

$$\nabla\times(\upsilon\nabla\times\boldsymbol{A})=J_s \qquad (22)$$

The conductivity of the rotor, which is the eddy current region in this case, is considered to be constant. This consideration ensures that the gradient of the electric scalar potential can be set to zero which has been shown by Rodger (1983). This gives the equation to be solved in the conducting region to be as given below.

$$\nabla\times(\upsilon\nabla\times\boldsymbol{A})+\sigma\frac{\partial\boldsymbol{A}}{\partial t}=0 \qquad (23)$$

As we have already mentioned, this study is a 'coupled 2D-3D' analysis of a solid rotor induction machine in a sense that the solution of the two dimensional study is used as the source in the three dimensional study. In this regard, the time-stepped state values of current densities in the stator conductors obtained from the two dimensional study in FCSMEK is used as the source current in the three dimensional as well as two dimensional study in the COMSOL Multiphysics™. So in the governing equation above that is Equation (13), the source current density term Js is used as the source to the machine which is accounted by forcing external current densities equal to the time-stepped three phase current densities in the stator slot obtained from the solution in FCSMEK.

The default 'magnetic insulation' boundary condition of COMSOL Multiphysics™ is used in the exterior boundary which sets the *z*-component of the magnetic vector potential to zero at the boundary

$$\boldsymbol{n} \times \boldsymbol{A} = 0 \qquad (24)$$

The continuity of the normal component of the flux density and the tangential component of the magnetic field strength is applied at the interface between the conducting and the non-conducting regions.

The geometry of the machine used for the simulation in COMSOL Multiphysics™ is built in commercially available CAD software which is already described in Section 3.3. To understand the two dimensional magnetic flux density distribution in the whole cross-section of the machine, the full pole pitch of the machine was used for the simulation. The geometry built in the CAD software was imported to COMSOL Multiphysics™. Since, the rotation of the rotor had to be modeled, we needed a geometry such that the rotor section could rotate. So, the imported geometry was re-processed to create two kind of geometrical entities. The first kind included the fixed geometrical parts like the stator core, stator slots and half of the radial length of the air gap and the second kind included the rotating geometrical parts like the rotor and the other half of the radial length of the air gap. The main reason for dividing the radial length of the air gap into two parts, a rotating and a stationary is to simplify the modeling of the rotation. The finalized geometry consisted of the assembly of these two parts. The interface between the rotating and the stationary geometry is used as the interface between the conducting and the non-conducting regions and a continuity pair boundary condition is applied in this interface which assures the continuity of the normal component of the flux density and the tangential component of the magnetic field.

The material used in the simulation was the same as that used in the FCSMEK. The material used for the stator core is Electrical Steel Sheet – Bochum STABOLEC 260-50 A and that for the rotor core is Construction Steel (Ovako 520 L) whose properties were predefined in FCSMEK and the same was prescribed in the material properties of the model. The stator core is a

magnetically non-linear medium and has zero conductivity whereas the rotor has an isotropic conductivity of a finite value and is also a magnetically non-linear medium. The magnetic non-linearity of the stator and the rotor core was applied by using the non-linear BH curve for both the core materials. The non-linear BH curve for the stator and the rotor core that are used in the model are shown in Figure 3.2 and 3.3 respectively and are the same as the ones used in FCSMEK.

The finite element mesh plays a vital role in the FEM calculation especially in the regard of both computational time and accuracy of the solution. Denser mesh results into higher number of unknown variables but gives a solution that is more likely to be accurate whereas a coarser mesh decreases the number of unknown variables and thus the computational time but the results are more likely to deviate from the accurate values. One another factor to be considered in meshing the finite element model for eddy current calculation is the maximum element size for the given skin depth. For a skin depth of 1 mm, the maximum size of the elements should be less than 0.5 mm in that region which has also been discussed by Lin (2009). In case of triangular elements the size of an element corresponds to the length of the longest edge of the triangle. The mesh built for the 2D simulation was such that the boundaries defined in the geometries are discretized (approximately) into mesh edges, referred to as boundary elements (or edge elements) by COMSOL Multiphysics™. The remaining geometry was meshed with first order triangular elements. The meshed geometry is shown in Figure 3.15 which is colored according to the quality of elements. A closer view of the mesh in the air gap is shown in Figure 3.16. The complete mesh consisted of 40970 elements.

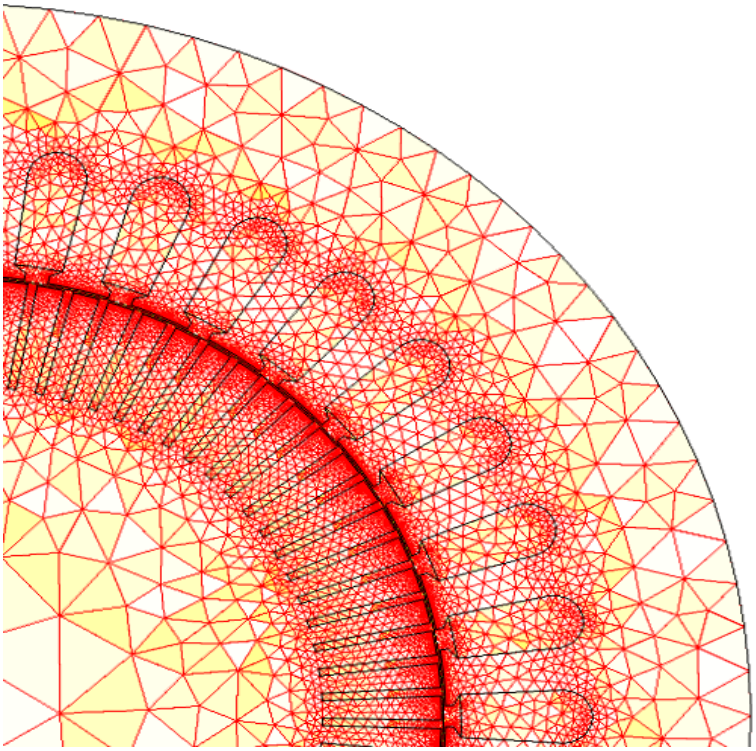

Figure 3.15 Part of the two dimensional mesh used in the 2D simulation with the commercial software COMSOL Multiphysics™.

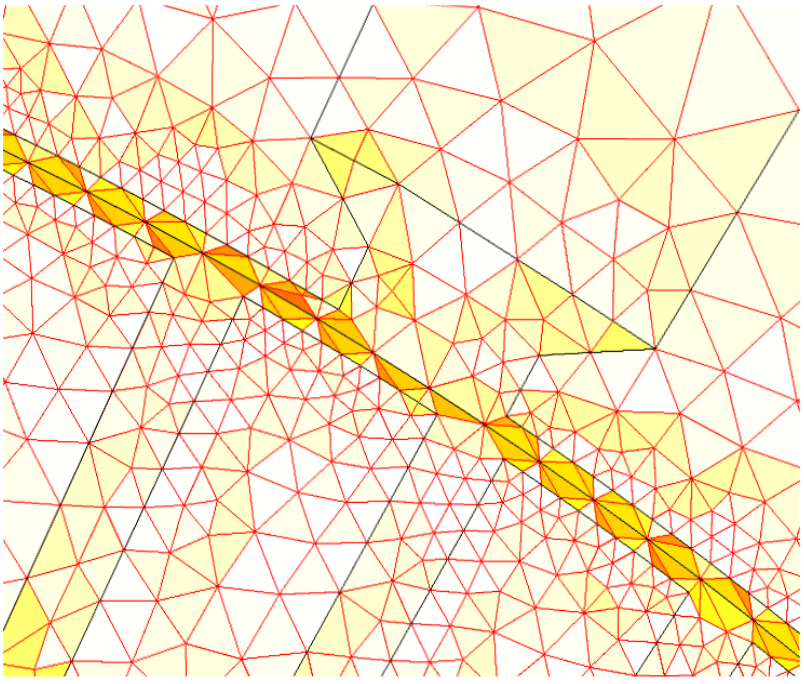

Figure 3.16 A closer view to the mesh near the air gap. The coloring is according to the element shape quality.

COMSOL Multiphysics™ offers a variety of solvers for time harmonic as well as time-stepping study. The time-stepping method is usually a very long process. The machine model should be simulated tens of periods of line frequency to achieve the steady state if the initial value field is assumed to be zero in time-stepping computation. So, the model is first simulated by the time harmonic method whose solution is then used as an initial state in the time stepping method. This method will take a considerably smaller computation time and the steady state can be achieved by simulating only few periods of line frequency.

One difficult aspect of the modeling of the rotating machinery is to model the rotation. One way to model the rotation is to consider the rotor as a quasi or pseudo-stationary object where it is fixed but the rotor conductivity is multiplied by the per unit slip *s* for modeling the rotation as described by Arkkio (1987). But this method is accurate only if the slip is 1. But Comsol has a feature where the mesh of the rotating domain can be deformed with a prescribed mesh displacement value. The main principle behind this feature is that we presribe a set of equations that defines the displacement of the mesh of the domain in which this feature has been used. So, in order to model the rotation of our model we used the 'Moving Mesh' feature of the COMSOL Multiphysics™ in the rotating part of the geometry that is the rotor and the equation for the mesh displacement in both x-axis and y-axis was defined such that

$$dx = \cos(2 * pi * \omega_s * t) * X - sin(2 * pi * \omega_s * t) * Y - X \qquad (25)$$

$$dy = sin(2 * pi * \omega_s * t) * X + cos(2 * pi * \omega_s * t) * Y - Y \qquad (26)$$

Where,

ω_s is the speed of the machine in *rps* at corresponding slip

X and Y are material frame coordinates.

The equations above ensure the displacement of the mesh of the rotating domain in each time step. The machine was rotated at 5% slip which makes $\omega_s = 23.75\, rps$. Thus the rotation in the machine is modeled by moving the mesh in each time step.

3.6.2 3D model

Though the two dimensional finite element analysis of the electromagnetic field is sufficient to study the approximate behavior of an electrical machine, some phenomena can be well accounted only when the three dimensional finite element analysis is done. So, a three dimensional model was built.

The three dimensional eddy current formulations have already been discussed in the earlier chapter. In our model, we have used the equations of the $\boldsymbol{A}-\phi,\boldsymbol{A}$ formulation where the magnetic vector potential $\boldsymbol{A}$ is calculated in both the conducting and the non-conducting region and the reduced electric scalar potential ϕ is calculated in the conducting region only. The governing equations used for the three dimensional formulation is the same as Equation (13) with vector $\boldsymbol{A}$ being a three dimensional vector. Even in this case, the reduced electric scalar potential ϕ is set to zero. Therefore the basic formulation used can be considered to be the magnetic vector potential formulation only. In the eddy current carrying region that is the conducting region, equation (21) is solved and in the eddy current free region where the eddy current density is assumed to be zero, equation (15) is solved.

A coupled 3D model was realized in a sense that the solution of the two dimensional study performed in the in-house software FCSMEK is used as the source in the three dimensional study. This was possible by using the time-stepped state values of three phase current densities in the stator conductors obtained from the solution in FCSMEK as the source current density in the three dimensional model in the COMSOL Multiphysics™. So the source current density term $\boldsymbol{Js}$ in the equation (13) for the 3-D model is used as the source current to the machine as it was done in the two dimensional study.

The default 'magnetic insulation' boundary condition of COMSOL Multiphysics™ is used in the exterior boundary which sets the tangential component of the magnetic vector potential zero at the boundary

$$\boldsymbol{n}\times\boldsymbol{A}=0 \qquad (27)$$

The continuity of the normal component of the flux density and the tangential component of the magnetic field is applied at the interface between the conducting and the non-conducting region.

The three dimensional geometrical model of the machine is also built in commercially available CAD software and the design process have been discussed in Section 3.3. The full pole pitch of the machine was used for the simulation. Due to the limited computing resources, the solution of the full length of the machine was not possible. So, to simplify the model only a quarter of the total axial length of the machine was simulated which significantly reduced the computation time. However, this simplification does not consider the machine end effects which are a major concern in 3-D eddy current problems. Therefore the result from this simulation is subjected to deviate to some extent from the accurate results. To account for the rotation of the rotor, the imported geometry was re-processed similarly as the two dimensional geometry described in the previous section. The finalized geometry consisted of the assembly of these two parts, a fixed part and a rotating part. The interface between the rotating and the stationary geometry is also used as the interface between the conducting and the non-conducting regions which means that the electric scalar potential is also calculated in the lower part of the air gap (the part included in the rotating geometry) and is equal to zero. A continuity pair boundary condition is applied in this interface which assures the continuity of the normal component of the flux density and the tangential component of the magnetic field.

The material used in the 3D model is the same as that used in FCSMEK and also for the 2-D simulation in COMSOL Multiphysics™. The material properties were predefined in FCSMEK and are prescribed in the material properties of the model in COMSOL Multiphysics™. The stator core is a magnetically non-linear medium and has zero conductivity whereas the rotor has an isotropic conductivity of a finite value and is also a magnetically non-linear medium. Since the conductivity of the rotor is constant throughout the rotor body, there will be no potential difference caused due to the electric charge in this region. Therefore the electric scalar potential in the equation (13) becomes zero. So, the formulation used here can be considered to be the magnetic vector potential formulation only. This

consideration decreases the number of dependent variables to be computed, thus reducing the computing time.

The magnetic non-linearity of the stator and the rotor core was applied by using the non-linear BH curve for both the core materials. The non-linear BH curve for the stator and the rotor core that are used in the model are shown in Figure 3.12 and 3.13 respectively.

Meshing a 3D model needs a special care and attention. An improper mesh will lead to inaccurate results and most of the time, COMSOL Multiphysics™ solver find it difficult to solve the models with such improper meshes. Our 3D model has a very thin air gap and meshing such thin domain requires good meshing skills. The maximum element size must be less than the size of the domain which creates a dense mesh of very small elements which may not lead to any solution as the solver cannot solve it. The 3D geometry was first meshed with a first order tetrahedral mesh. The 3D geometry meshed with the tetrahedral mesh is shown in Figure 3.16. The mesh resulted in too high number of degree of freedoms to be solved and was impossible to solve by the computer due to limited computer memory (8, 16 or 32 GB).

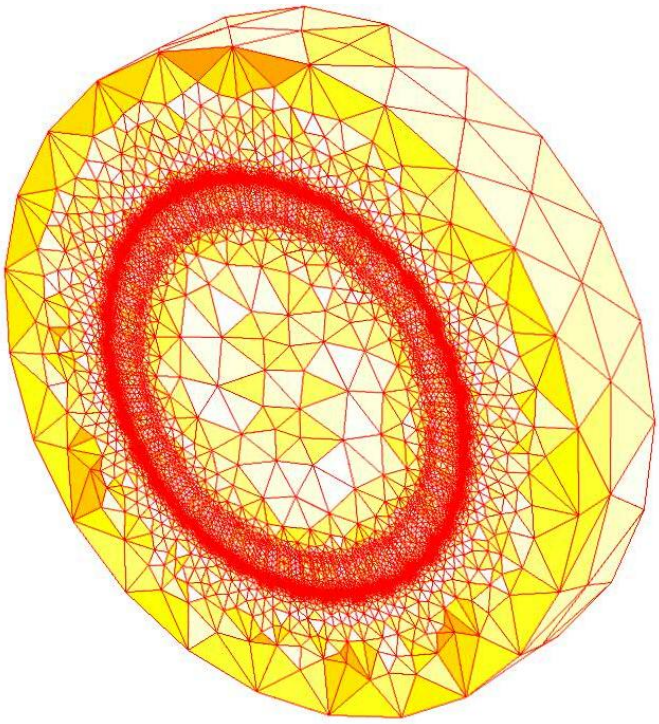

Figure 3.17 Tetrahedral mesh in 3D geometry

Therefore an alternative way of meshing the 3D geometry was considered. In this method, the 3D mesh was created in such a way that one of the axial cross-sectional faces of the machine was meshed with a triangular mesh which was then swept across the axial length to the other face. The complete mesh consisted of 32200 elements which resulted into lower DoFs relative to the tetrahedral mesh which had 740013 elements. The complete swept mesh is shown in Figure 3.18.

The same solver used for the 2D simulation in COMSOL Multiphysics™ described earlier is also used for the 3D simulation. To avoid long computation time, first the time-harmonic study is performed whose solution is then used as an initial state in the time stepping method. A moving mesh is used in the rotating

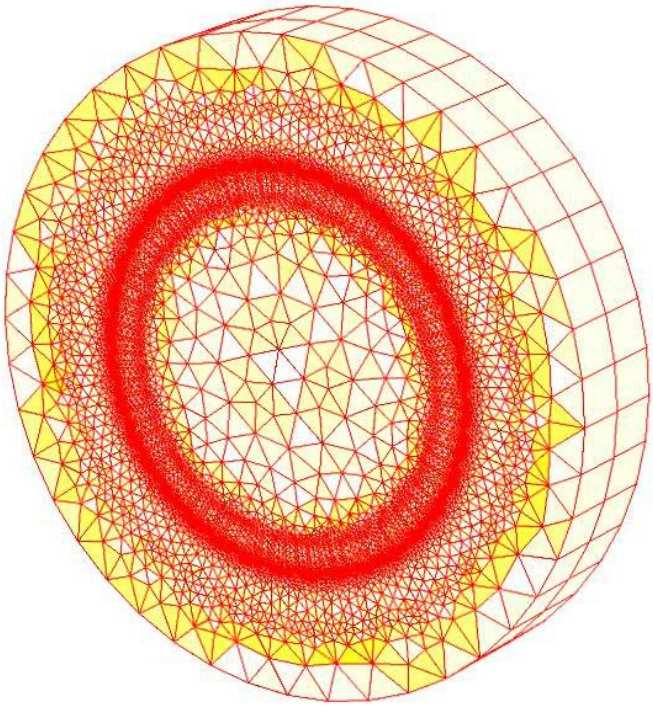

Figure 3.18 Prism Mesh created by sweeping the triangular mesh

domain to realize the rotation of the rotor. The displacement of the mesh in x and y axis are the same as that in Equation (25) and (26) and that in z-axis is zero which is shown in Equation (28). These equation are prescribed in the rotating domain.

$$dz = 0 \qquad (28)$$

X , Y and Z are material frame coordinates.

These ensure the displacement of the three-dimensional mesh of the rotating domain in each time step. The machine was rotated at 5% slip which makes $\omega_s = 23.75\ rps$. Thus the rotation in the machine is modeled by the same method as in the two-dimensional model by moving the mesh in each time step.

~ CHAPTER 4 ~

RESULTS AND DISCUSSIONS

Synopsis

This Chapter contains the results of both the two-dimensional and three-dimensional study carried out in the COMSOL Multiphysics™. Different plots and graphs are produced from the results and are presented in this chapter. Their findings are also discussed in this chapter.

4.1 Results from 2-D Simulation

The two dimensional model built in COMSOL Multiphysics™ is described in Section 3.5.1. Both time-harmonic and time dependent study is performed on the model. The end-effect of the machine is neglected. The two dimensional finite element mesh is shown in Figure 3.14 and 3.15. The mesh consisted of 20416 elements of type including triangular, edge and vertex elements. The number of DoFs solved was 20932. Five periods of the line frequency with four hundreds time-steps per period was simulated. The total computational time for the time-dependent study of the two dimensional model with 20932 DoFs was 4134 seconds. The simulation was performed on a computer with Intel® Core(T)2 Quad CPU with 8 GB RAM.

The flux density distribution obtained from the time-dependent study is shown in Figure 4.1. We can see that in the stator more flux is concentrated in the stator teeth near the poles and in the stator yoke around the inter-polar regions. In the rotor, the flux is more concentrated near to the surface of the rotor. This is because of the fact that the flux penetration into the conducting rotor material causes the eddy currents which again tends to prevent the flux penetration.

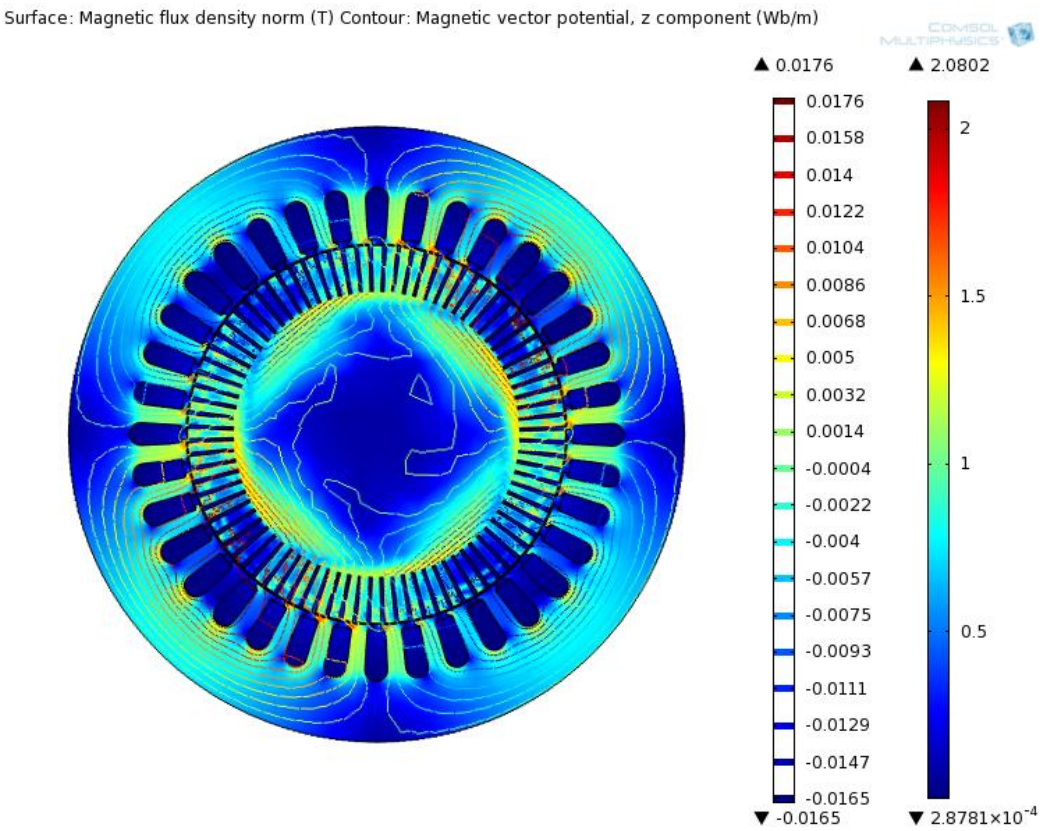

Figure 4.1 Magnetic flux density distribution and the flux lines as computed with TSA in the COMSOL Multiphysics™ software.

The axial slits in the solid rotor form a path for the eddy currents to flow from one rotor end to the other through the rotor teeth between the slits. A circulating magnetic flux is created by the currents that flow through the rotor teeth. So, the flux lines make a magnetic spiral or curl shape in the solid rotor with axial slits. The resulting flux lines are shown along with the magnetic flux density distribution in Figure 4.1.

Figure 4.2 shows the eddy currents density that is induced in the solid rotor resulting from the time-dependent study. We can see that the induced currents are mainly distributed in the rotor teeth and penetrate to a very low level inside the rotor. This may be due to small skin depth of the rotor. It can also be understood from the same figure that the eddy current is flowing along the axial direction that is along the z-direction. From the figure, only the distribution of eddy currents can be seen, but the flow of the current can be well visualized in the three dimensional model.

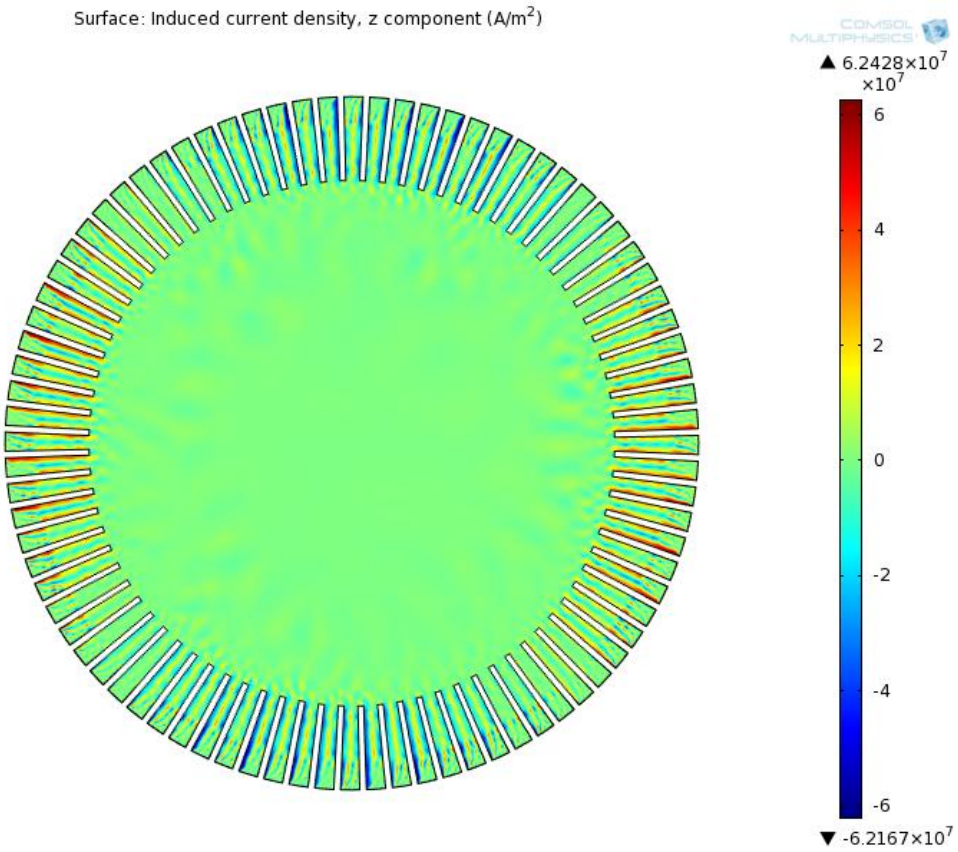

Figure 4.2 Eddy current density distribution

The time variation of the torque calculated from the 2-D simulation with COMSOL Multiphysics™ is shown in the figure 4.3.

The average air gap torque of the machine is higher than that calculated in FCSMEK. The electromagnetic torque is calculated using the Maxwell's stress tensor and is given by the surface integral over the closed surface S located in the air gap.

$$\boldsymbol{T} = \oint \boldsymbol{r} \times \boldsymbol{\sigma}.dS \qquad (29)$$

Where, $\boldsymbol{\sigma}$ is the Maxwell's stress tensor and $\boldsymbol{r}$ is the position vector directed from the rotor origin to the point of calculation. In 2-D model the surface integral is reduced to the line integral along the air gap.

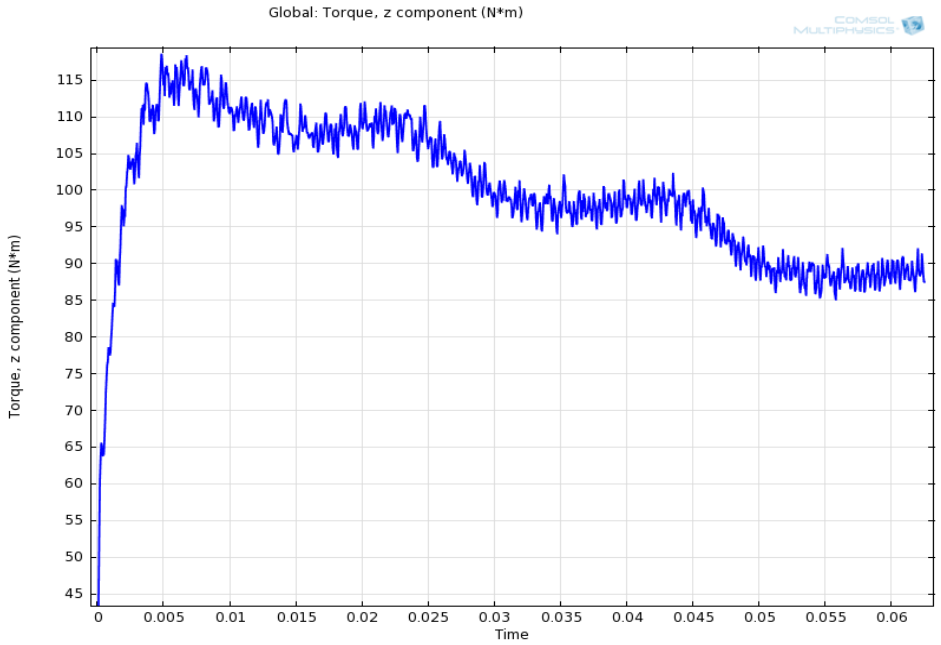

Figure 4.3 Torque variation resulting from 2-D simulation in COMSOL Multiphyscis™

4.2 Results from 3-D Simulation

The three dimensional model built in COMSOL Multiphysics™ is described in Section 3.5.1. Both time-harmonic and time dependent study is performed on the 3-D model too. Taking both the active region and the end region of the machine into consideration for the model would increase the complexity of the problem. So, only the active region of the machine was taken into account and the end-effect of the machine is neglected. This will however produce a result that is subjected to deviate to some extent from the accurate result as discussed in earlier chapter. The 3-D mesh is shown in Figure 3.17. The complete mesh consisted of 32200 elements which include triangular, prism, quadrilateral, edge and vertex elements. To reduce the number of unknown variables, only one-fourth of the axial length of the machine was simulated. The number of Degree of Freedoms solved was 90622. Five periods of the line frequency with four hundreds steps per period were simulated. The total computational time for the time-dependent study of the three dimensional model in a computer with Intel® Xeon® CPU with 16 GB RAM for 90622 DoFs was 19853 seconds.

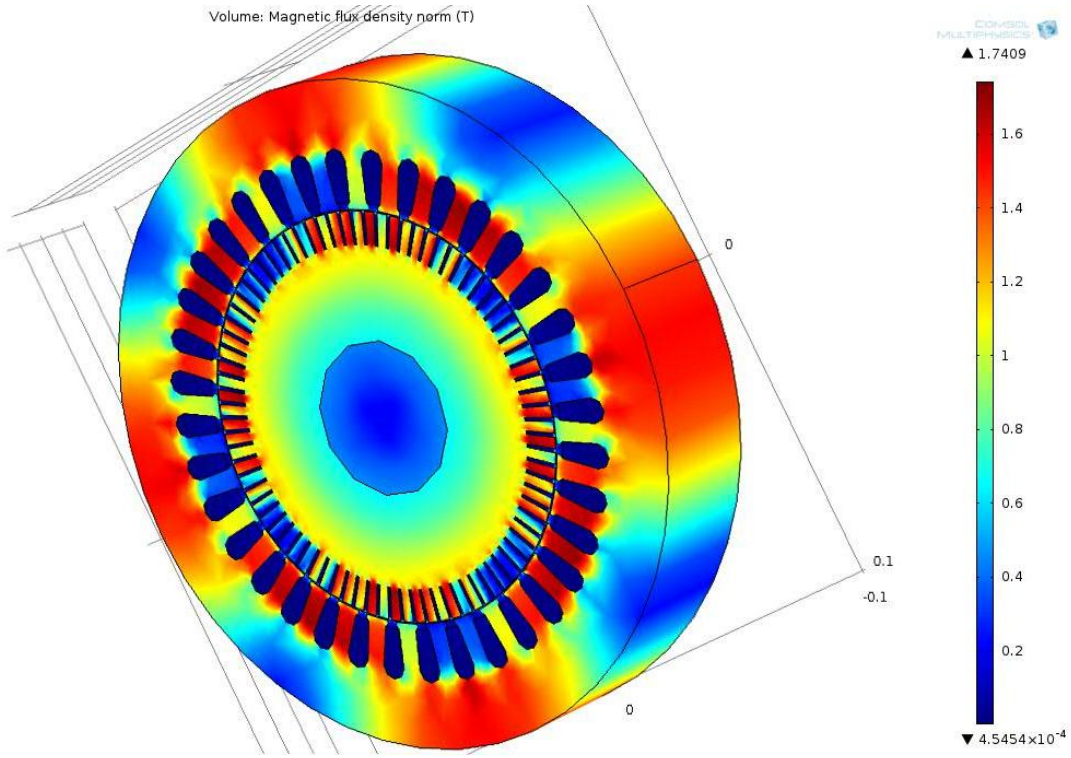

Figure 4.4 Three-dimensional flux density distribution computed with the 3D model in COMSOL Multiphysics™.

The three-dimensional flux density distribution in the machine is shown in Figure 4.4. The flux seems to be concentrated in the stator yoke in the inter-polar region and in the stator teeth near the poles in the stator. In the rotor, the flux is more concentrated near the surface of the rotor because of the fact that the induced current in the conducting rotor tends to oppose the flux penetration into it. The result of the 3-D simulation, in terms of the computed magnetic flux density is quite different. We can see that the flux density is quite high compared to the 2-D model.

The flow of the eddy currents through the rotor bars between the slits from one end of the rotor to the other end can be clearly visualized in the three-dimensional model. The eddy current density distribution and the flow of current from one end of the rotor to the other can be seen from Figure 4.5.

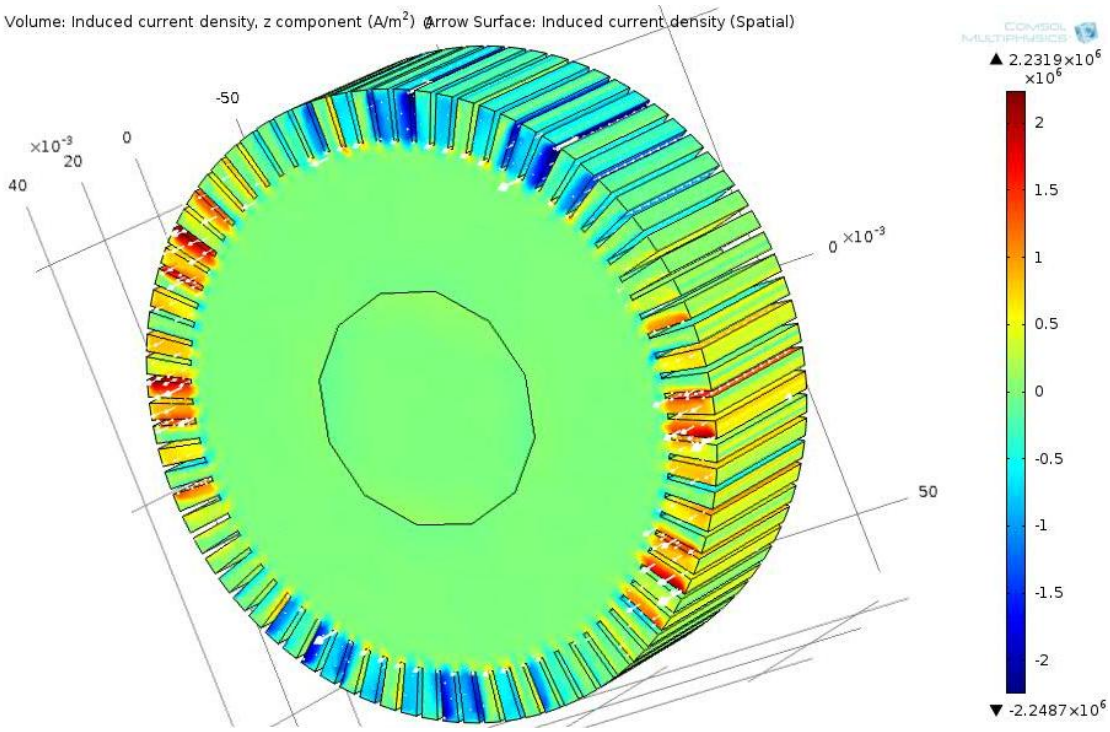

Figure 4.5 Eddy current density distribution and the flow of eddy currents (z-component)

A closer view of the flow of the eddy currents is presented in Figure 4.6. Currents circulate mainly through the surface of the rotor bars. It flows from one end to the other at one pole of the machine and returns back similarly from the other end at the adjacent pole. However, the looping of the currents at the end faces of the rotor could not be accurately modeled.

The torque calculated from the 3-D simulation is plotted in Figure 4.7. The torque is calculated using the Maxwell's stress tensor.

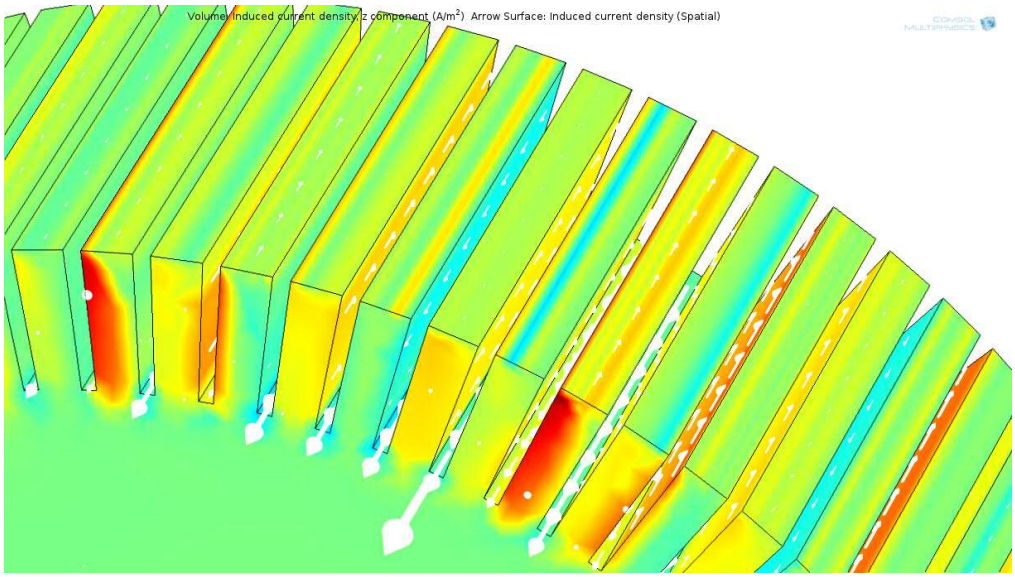

Figure 4.6 Computed z-component of the Eddy Currents.

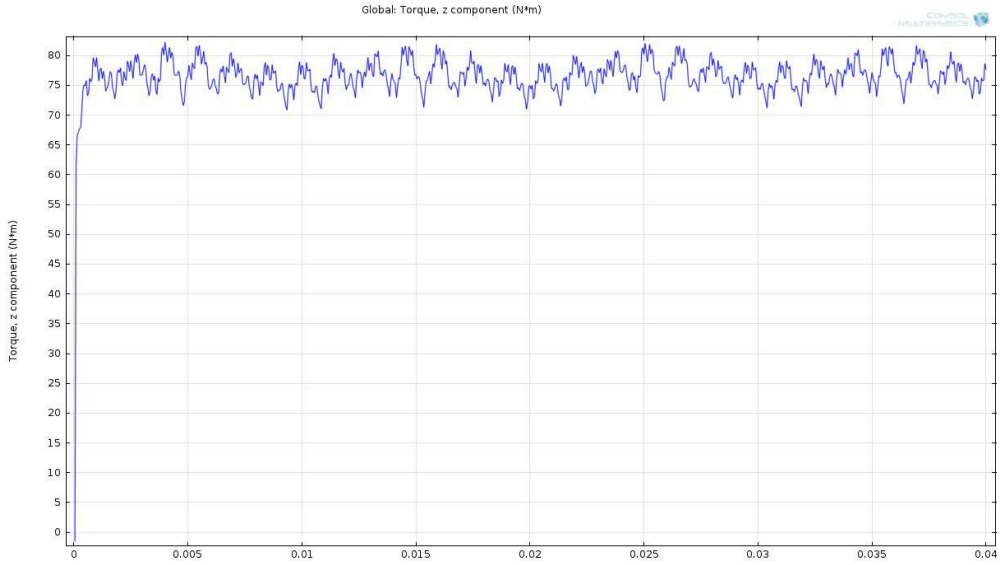

Figure 4.7 Torque variation resulting from 3-D simulation in COMSOL Multphysics™

~ CHAPTER 5 ~

CONCLUSION

The finite element method was used to compute the eddy currents in both two dimensional and the three dimensional model of a solid rotor induction machine. A three phase, 50 Hz, 380 V, star connected, 7.5 kW solid steel rotor induction machine was considered for the study. At first the two dimensional model of the machine was simulated in the in-house software FCSMEK. The eddy current was computed and the distribution of the eddy currents in the rotor teeth and rotor surface was studied. A three dimensional finite element model of the same machine was built in commercial software Comsol Multiphysics™. But before modeling the three dimensional model, a two dimensional model was built in Comsol Multiphysics™ as an initial approach to use the software and be able to compare the two different 2D approaches. Both the two dimensional and three dimensional model in Comsol Multiphysics™ was built in such a way that they were coupled with the model in FCSMEK. The original idea behind the coupled model was such that the computed magnetic vector potential in the rotor surface from the 2-D simulation in FCSMEK would be stored and then used as an initial value in one of the rotor surface in the 3-D model in Comsol Multiphysics™ and then extruded along the axial length of the machine with a suitable interpolation. Since, only the study of the rotor would be sufficient to accurately model the eddy currents, without the need of the 3-D model of the stator, this type of coupled model would have a great advantage in terms of simplicity and the reduction of computational time.

This kind of coupled model was tried to build in Comsol Multiphysics™, but the nodal values of the magnetic vector potential could not be transferred to the nodes of the rotor mesh in Comsol Multiphysics™. Comsol Multiphysics™ did not support any alteration of its finite element mesh externally. So, an alternative way was chosen. A coupled model was however realized, but the transferred variable was the time-stepped stator winding current density. The time-stepped solution of

the stator winding current density was used as a source to the windings in both the 2-D and the 3-D model in Comsol Multiphysics™. The $\boldsymbol{A} - \phi$ formulation was used for the eddy current calculation. The physical model of the machine was built in a CAD software called SolidWorks™ and then exported to Comsol Multiphysics™. The results from all the simulations are shown in the earlier chapters.

Although it was expected that the coupled model reduces the computational time,the results did not match the expectations. The results from the FCSMEK and Comsol Multiphysics™ differ quite considerably, especially in terms of the torque. The magnetic flux density distribution in the machine computed from the 2-D model in Comsol Multiphysics™ is similar to the flux density distribution computed from FCSMEK. However, the average flux density in the air gap is comparatively lower than that calculated in FCSMEK. The magnetic flux density computed in the 3-D model is slightly higher than that in the 2-D models. The advantage of 3-D model is that the field distribution in the actual machine can be visualized. The eddy current distribution in the rotor surface is plotted from the results of each simulation. From the 2-D plot of the eddy current distribution, it can be seen that the eddy current are mostly distributed in the rotor teeth. The eddy currents circulate through the surface of the rotor teeth, which can be clearly noticed in the 3-D eddy current plots. The eddy current flows from one end of the rotor to the other end through the axial surface of the rotor teeth and the radial surface provides the return path for it. However, the looping of the current near the end surface of the rotor could not be obtained. This is the major limitation of the model built in COMSOL Multiphysic™ in this thesis. The torque calculation in COMSOL Multiphysics™ when compared to that in FCSMEK differs quite considerably. It is seen that the torque calculated in both 2-D and the 3-D model in COMSOL Multiphysics™ is considerably high than that calculated in FCSMEK, around 2.5 and 2.2 times.

Thus, the eddy current was computed using both 2-D and 3-D Finite Element Method. A coupled model was studied by using the solution from results of 2-D simulation in the in-house software as a source to the 2-D and 3-D model in commercial software COMSOL Multiphysics™. Since the experimental results

for the machine were not available, the simulated results could not be validated. The major limitation of the coupled model discussed here in this thesis is that the looping of the eddy currents near the end region of the rotor could not be obtained. So, this model can be given additional work in future to address this limitation. Also the computational time of the coupled model was more than expected.

References:

A. Arkkio, (1987). Analysis of Induction Motor Based on the Numerical Solution of the Magnetic Field and Circuit Equations. *Acta Polytechnica Scandinavica,* 59

A. Arkkio, (1990). Finite Element Analysis of Cage Induction Motors fed by Static Frequency Converters, *IEEE Trans. Magn.*, 26(2):2-5.

B. Brunelli, D. Casadei, U. Reggiani, G. Serra, (1983). Transient and Steady-State Behavior of Solid Rotor Induction Machines, *IEEE Trans. Magn.,* 19(6):2650-2654.

B. Davat, Z. Ren, M. Lajoie-Mazenc, (1985). The Movement in Field Modeling. *IEEE Trans. Magn.* 21(6):2296-2298.

D. Rodger, (1983). Finite Element Method for Calculating Power Frequency 3-Dimensional Electromagnetic Field Distributions. *In Proc. IEE, Science, 130*

J. D. Jackson, (1999). *Classical Electrodynamics*. 3rd ed. New York, NY, John Wiley and Sons Inc.

J. Gieras, (1995). Solid-Rotor Induction Motor Design, pages 293-298. In *Engelmann, R., Middendorf, W.* Handbook of Electric Motors, Marcel Dekker Inc., New York.

J. F. Gieras, J. Saari, (2010). Performance Calculation for a High Speed Solid-Rotor Induction Motor. In Proc. *36th Annual Conference on IEEE Industrial Electronics Society*, pages 1748-1753, Glendale, AZ, USA.

J. Huppunen, (2004). High-Speed Solid-Rotor Induction Machine – Electromagnetic Calculation and Design. *Doctoral Dissertation, Lappeenranta University of Technology*, Lappenranta, Finland.

J. Luomi, (1993). *Finite Element Methods for Electrical Machines*. Lecture Notes, Chalmers Universtiy of Technology, Göteborg, Sweden.

M. J. Balchin, J. A. M. Davidson, (1983). 3-Dimensional Eddy-Current Calculation by the Network Method Formulation Using Magnetic Scalar Potential for Nonconducting Regions. In *Proc. IEE, A Physical Science, Measurement and Instrumentation, Management and Education, Reviews*, *130*(2):88.

M. J. Islam, A. Arkkio, (2008). Time-Stepping Finite-Element Analysis of Eddy Currents in the Form-Wound Stator Winding of a Cage Induction Motor Supplied from a Sinusoidal Voltage Source. In *Proc. IET Electrical Power Applications*, 2(4):256-265

O. Biro, K. Preis, (1989). On The Use of the Magnetic Vector Potential in the Finite-Element Analysis of Three-Dimensional Eddy Currents. *IEEE Trans. Magn*, 25(4):3145-3159.

O. Biro, K. Preis, (1990). Finite Element Analysis of 3-D Eddy Currents. *IEEE Trans. Magn.*, 26(2):418-423.

P. Dziwniel, F. Piriou, J. P. Ducreux, P. Thomas, (1999). A Time-Stepped 2D-3D Finite Element Method for Induction Motors with Skewed Slots Modeling. *IEEE Trans. Magn.*, 35(3):262-1265.

P. J. Leonard, D. Rodger, (1988). Finite Element Scheme for Transient 3D Eddy Current Analysis. *IEEE Trans. Magn.*, 24:90.

S. L. Ho, Niu. Shuangxia, W. N. Fu, (2010). A Novel Solid-Rotor Induction Motor with Skewed Slits in Radial and Axial Directions and Its Performance Analysis Using Finite Element Method. *IEEE Trans. App. Superconductivity*, 20(3):1089-1092.

S. Kanerva, (2001). Data Transfer Methodology Between a FEM Program and a System Simulator. In *Proc. 5th Int. Conf. Electrical Machines and Systems.* Vol(2):1121-1124).

T. Aho, J. Nerg, J. Pyrhonen, (2006). The Effect of the Number of Rotor Slits on the Performance Characteristics of Medium-Speed Solid Rotor Induction motor. In *Proc. 3rd IET Int. Conf. Power Electronics, Machines and Drives*, pages 515-519, Dublin, Ireland.

T. Kikuchi, T. Kenjo, (1997). A unique Desk-top Electrical Machinery Laboratory for the Mechatronics Age. *IEEE Trans. Education*, 40(4).

T. Yang, L. Zhou, W. Jiang, (2008). Calculation of Eddy Current Losses in a Solid-Rotor Cage Induction Motor by Finite Element Analysis. In *Proc. Int. Conf. Electrical Machines and Systems*, pages 3656-3659, Wuhan, China.

W. Muller, A. Knoblauch, (1985). A Method for Numerical Calculation of 3D Eddy-Currents. *IEEE Trans. Magn.*, 21(6).

APPENDIX

APPENDIX A: MATLAB Codes used to read the *cim.fedat* file of FSCMEK

```
function f = readCimFedat(file)
% Read FEM data from cim.fedat

    if nargin == 0
      clc;
      file = 'T:\results';
    end;
    if file(end) == '\'
      file = [file 'cim.fedat'];
    end;

    fid = fopen(file);
%    fgetl(fid);
%    luvut = fscanf(fid, '%d',5);

    % Number of nodes and elements
    maxnp = luvut(1);
    maxel = luvut(2);
    nfe   = luvut(3);
    npm   = luvut(4);
    ndb   = luvut(5);

    % HPER and pituus
    luvut = fscanf(fid, '%f', 2);
    hper  = luvut(1);
    pituus = luvut(2);
    fgetl(fid);

    % Read FFE table
    line = fgetl(fid);
    luvut = sscanf(line, '%f');
    ffe= [];
    while length(luvut) < 6
      ffe(end+1,1:5) = luvut(1:5);
      line = fgetl(fid);
      luvut = sscanf(line, '%f');
      ffe(end,6:9) = luvut(1:4);
      line = fgetl(fid);
      luvut = sscanf(line, '%f');
    end;

    % Node coordinates
    cordx(1) = luvut(2);
    cordy(1) = luvut(3);
    a(1)     = luvut(4);
    ibc(1)   = luvut(end);
    luvut = fscanf(fid, '%d%f%f%f%f%d', [6 maxnp-1])';
    cordx(2:maxnp) = luvut(:,2);
    cordy(2:maxnp) = luvut(:,3);
    a(2:maxnp)     = luvut(:,4);
    ibc(2:maxnp)   = luvut(:,end);
```

```
% Elements
for i = 1 : maxel
  luvut = fscanf(fid, '%d', 2);
  nodel(i) = luvut(2);
  nop(i,:) = fscanf(fid, '%d', nodel(i));
  imat(i) = fscanf(fid, '%d', 1);
end;
rivi = fgetl(fid);

% Number of air gap elements and rotor angle
luvut = fscanf(fid, '%f',2);
nag = luvut(1);
alfa = luvut(2);

% Air gap element
luvut = fscanf(fid, '%*d%d%f', [2 nag+2])';
ngap = luvut(:,1);
fgap = luvut(:,2);
luvut = fscanf(fid, '%d', 4);
igap = luvut(1);
maxg = luvut(2);
mexg = luvut(3);
nstb = luvut(4);

% PAR tables
luvut = fscanf(fid, '%f', [4 100])';
par = luvut(:,2);
ipar = luvut(:,3);
spar = luvut(:,4);
fclose(fid);

% Calculate element areas
for k = 1 : maxel
  x = cordx(nop(k,1:3));
  y = cordy(nop(k,1:3));
  ala(k) = 0.5*abs(det([x; y; 1 1 1]));
end;

lse = ipar(51);                    % Last stator element
lre = ipar(52);                    % Last rotor element
lsn = max(max(nop(1:lse,:)));      % Last stator node
lrn = max(max(nop(lse+1:lre,:)));  % Last rotor node

% Output
f.ffe    = ffe;
f.maxnp  = maxnp;
f.maxel  = maxel;
f.cordx  = cordx';
f.cordy  = cordy';
f.cord   = [cordx' cordy'];
f.nodel  = nodel;
f.nop    = nop;
f.imat   = imat';
f.a      = a';
f.alfa   = alfa;
f.par    = par;
f.ipar   = ipar;
f.spar   = spar;
f.ibc    = ibc;
```

```
f.ala    = ala;
f.lse    = lse;
f.lre    = lre;
f.lsn    = lsn;
f.lrn    = lrn;
f.nag    = nag;
f.ngap   = ngap;
f.fgap   = fgap;
f.igap   = igap;
f.maxg   = maxg;
f.mexg   = mexg;
f.nstb   = nstb;
f.nfe    = nfe;
f.npm    = npm;
f.ndb    = ndb;
f.hper   = hper;
f.pituus = pituus;
```

APPENDIX B: MATLAB Code to read the *cimtd.tulos* file of FCSMEK

```
clear all
file='T:\cimtd.tulos';
id=fopen(file,'r');
for i=1:2
fopen(id);
end
td=fread(id,'%e ,%e ,%e ,%e ,%e ,%e ,%e ,%e ,%e ,%e ,%e ,%e ,%e
,',[14 inf]);
td=td';
n=size(td,1);
t=td(n/3:n,1);
w=td(n/3:n,2);
T=td(n/3:n,3);
I123=td(n/3:n,4:6);
Uv=td(n/3:n,7:9);
V=td(n/3:n,10:12);
P=td(n/3:n,13:14);
I=I123;
subplot(2,2,1); plot(t,I123); xlabel('Time (ms)'); title('Line
currents'); grid on;
subplot(2,2,2); plot(t,V);xlabel('Time (ms)');title('Line
voltages');grid on;
subplot(2,2,3); plot(t,T);xlabel('Time (ms)');title(['Torque
average: ' num2str(mean(T),'%g')]);grid on;
subplot(2,2,4); plot(t,Uv);xlabel('Time (ms)');title('Phase
voltages');grid on;
```